Title: Chickpea NCR13 disulfide cross-linking variants exhibit profound differences in antifungal activity and modes of action

Authors: James Godwin[a,1], Arnaud Thierry Djami-Tchatchou[a,1], Siva L. S. Velivelli[a], Meenakshi Tetorya[a], Ravi Kalunke[a], Ambika Pokhrel[a], Mowei Zhou[c,2], Garry W. Buchko[c,d], Kirk J. Czymmek[a,b], and Dilip M. Shah[a,3]

Author Affiliations:

[a]Donald Danforth Plant Science Center, St Louis, MO. 63132, USA

[b]Advanced Bioimaging Laboratory, Donald Danforth Plant Science Center, St Louis, MO. 63132, USA

[c]Earth and Biological Sciences Directorate, Pacific Northwest National Laboratory, Richland, WA 99354, USA

[d]School of Molecular Biosciences, Washington State University, Pullman, WA 99164, USA

1. These authors contributed equally to the manuscript.

2. Current address: Department of Chemistry, Zhejiang University, 866 Yuhangtang Road, Hangzhou, Zhejiang 310058, China

3. Corresponding Author:

Correspondence and requests for materials should be addressed to D.M.S. (Email: dshah@danforthcenter.org)

Abstract

Small cysteine-rich antifungal peptides with multi-site modes of action (MoA) have potential for development as biofungicides. In particular, legumes of the inverted-repeat lacking clade express a large family of nodule-specific cysteine-rich (NCR) peptides that orchestrate differentiation of nitrogen-fixing bacteria into bacteroids. These NCRs can form 2 or 3 intramolecular disulfide bonds and a subset of these peptides with high cationicity exhibits antifungal activity. However, the importance of intramolecular disulfide pairing and MoA against fungal pathogens for most of these plant peptides remains to be elucidated. Our study focused on a highly cationic chickpea NCR13, which has a net charge of +9 and contains six cysteines capable of forming three disulfide bonds. NCR13 expression in *Pichia pastoris* resulted in formation of two peptide folding variants, NCR13_PFV1 and NCR13_PFV2, that differed in the pairing of two out of three disulfide bonds despite having an identical amino acid sequence. The NMR structure of each PFV revealed a unique three-dimensional fold with the PFV1 structure being more compact but less dynamic. Surprisingly, PFV1 and PFV2 differed profoundly in the potency of antifungal activity against several fungal plant pathogens and their multi-faceted MoA. PFV1 showed significantly faster fungal cell-permeabilizing and cell entry capabilities as well as greater stability once inside the fungal cells. Additionally, PFV1 was more effective in binding fungal ribosomal RNA and inhibiting protein translation *in vitro*. Furthermore, when sprayed on pepper and tomato plants, PFV1 was more effective in reducing disease symptoms caused by *Botrytis cinerea*, causal agent of gray mold disease in fruits, vegetables and flowers. In conclusion, our work highlights the significant impact of disulfide pairing on the antifungal activity and MoA of NCR13 and provides structural framework for design of novel, potent antifungal peptides for agricultural use.

Author Summary

Fungal pathogens cause significant pre-harvest and post-harvest losses of crop yield, making them a serious biological threat to global food security. Chemical fungicides are effective in controlling fungal diseases across various crops. However, rapid evolution of fungal pathogen resistance to single-site chemical fungicides in agriculture has created an urgent need for development of safe, sustainable, and cost-effective multi-site fungicides. Nodule-specific cysteine-rich (NCR) peptides expressed in the inverted-repeat lacking clade legume plants exhibit potent antifungal activity; however, their modes of action (MoA) are poorly understood. Particularly, the specific contribution of disulfide pairing to the potency and spectrum of antifungal activity against fungal plant pathogens and MoA of these peptides remains to be identified. Chickpea NCR13 expressed in *P. pastoris* generates two peptide variants that differ in their disulfide cross-linking pattern. These variants exhibit striking differences in their three-dimensional structures and potency of antifungal activity against multiple fungal pathogens and MoA. They also differ in their ability to confer resistance to gray mold in pepper and tomato plants. Our study highlights the major impact a specific pattern of disulfide pairing can have on the *in vitro* and *in planta* antifungal activity of an NCR peptide.

Introduction

The management of fungal diseases using chemical fungicides is one of the mainstays of modern agriculture. Unfortunately, modern fungicides that have a single site mode of action (MoA) are losing their effectiveness owing to an increase in development of fungal resistance (1). A major limitation in fungicide development is finding molecules with novel structures and multi-site MoA to mitigate evolution of resistance.

Plants express many antimicrobial peptides that are vital components of the innate immune system and act as a first line of defense against bacterial and fungal pathogens (2, 3). Moreover, plants express a multitude of cationic antifungal peptides differing in structure and sequence (4). They are versatile, have large sequence space, and can be tuned for broad-spectrum antifungal activity against plant fungal pathogens. Thus, cationic antimicrobial peptides represent promising templates for a new generation of fungicides with broad action against fungal pathogens (5).

Several antifungal peptides expressed in plants are cysteine-rich with a characteristic number of cysteine-residues at conserved positions and exhibit high degree of sequence diversity (4, 6). Defensins and defensin-like peptides are the best characterized examples of cysteine-rich peptides employed by plants to combat fungal pathogens (7-9). Legumes of the inverted repeat-lacking clade (IRLC) express many nodule-specific cysteine-rich (NCR) defensin-like peptides that cause differentiation of nitrogen-fixing bacteria to bacteroids. In *Medicago truncatula* and chickpea, terminal differentiation process is orchestrated by 639 and 63 nodule-specific cysteine-rich (NCR) peptides respectively, with conserved cysteine motifs (10). NCRs cause bacterial genome endoreduplication, changes in transcription and translation, and induction of morphological changes leading to the formation of bacteroids with unique morphology (8, 11-13). Each NCR is synthesized as a precursor protein containing an N-terminal signal peptide and a C-terminal mature

97 peptide. Several NCRs in each legume are cationic with a net charge ranging from +3 to +11 and
98 rich in hydrophobic residues, dual hallmarks of defensin-like antimicrobial peptides (10, 14).
99 Large landscape of natural NCRs from IRLC legumes offer an unprecedented opportunity for
100 discovery of the novel antimicrobial functions in plants. Several NCR peptides exhibiting
101 antibacterial activity against Gram-negative and Gram-positive bacteria have so far been identified
102 (15-18). Another report detailed the evaluation of 19 cationic *M. truncatula* NCRs for their ability
103 to inhibit the growth of a human fungal pathogen *Candida albicans*. Of these, nine with a net
104 charge above +9 inhibited the growth of this pathogen at concentrations ranging from 1.5 to 10.5
105 μM (14). Previously, we reported *M. truncatula* NCR044 having broad-spectrum antifungal
106 activity and multi-faceted MoA. In addition, when sprayed on leaf surfaces of tomato and
107 *Nicotiana benthamiana* plants, NCR044 conferred resistance to the gray mold disease caused by
108 the fungal pathogen *B. cinerea* (19).

109 NCRs exhibit diverse primary sequences and net charges, with a notable conserved feature
110 being the presence of four or six conserved cysteine residues. These cysteines form intramolecular
111 disulfide bonds which enhance the stability of the peptides (10, 20). The influence of cysteines and
112 disulfide cross-linking on the structure and function of *M. truncatula* NCR247 and NCR169, each
113 containing four cysteines, has been previously investigated. Four conserved cysteines and disulfide
114 cross-linking had major influence on the symbiotic activities of NCR247 tested against
115 *Sinorhizobium meliloti* (21, 22). NCR169 produced two structurally distinct disulfide variants that
116 exhibited differences in phospholipid binding and antibacterial activity (23). However, the
117 significance of disulfide cross-linking for the structures, antifungal activity, and MoA of majority
118 of NCRs is poorly understood.

119 In this study, we show that a highly cationic chickpea NCR13 peptide expressed in *Pichia*
120 *pastoris* forms two structurally unique disulfide variants despite having an identical amino acid
121 sequence. Interestingly, these two variants exhibited distinct differences in their antifungal potency
122 against economically important plant fungal pathogens. NCR13 disulfide variants displayed
123 notable differences in fungal cell entry, cell permeabilization, stability and MoA against the fungal
124 pathogen *B. cinerea*. While both disulfide variants reduced gray mold disease symptoms by spray
125 application on the leaves of pepper and tomato plants, the NCR13 variant with potent *in vitro*
126 antifungal activity was more effective in controlling the disease *in planta*. Our study reveals the
127 remarkable impact of disulfide cross-linking on the structure-activity relationships and MoA of an
128 antifungal defensin-like NCR peptide.
129

130 **Results**

131 **Chickpea NCR13 is expressed in *P. pastoris* as two peptide folding variants differing in**
132 **disulfide pairing**

133 In chickpea, NCR13 is one of 63 predicted NCR peptides expressed only in nodules
134 undergoing differentiation during symbiosis (10, 24). NCR13 is a 32-residue peptide with six
135 cysteines predicted to form three disulfide bonds (Fig 1A). Two other homologs of this peptide,
136 NCR07 and NCR15, are also expressed in chickpea nodules with highly conserved cysteine
137 residues (Fig 1A). No other IRLC legumes express NCRs with significant homology to NCR13.
138 NCR13 has 66.6% and 48.4% sequence identity with NCR15 and NCR07, respectively, carrying
139 a net charge of +8 and a hydrophobic amino acid content of 28%, hallmark features of a potential
140 antifungal peptide (Fig 1B).

To investigate the antifungal properties of the NCR13 peptide, it was expressed in a heterologous *Pichia pastoris* system. The peptide was secreted into the growth medium and purified using the cation exchange chromatography. When the NCR13 peptide was subjected to C18 reverse-phase high-performance liquid chromatography (HPLC), we consistently observed two peaks (Fig 1C). In contrast, chemically synthesized NCR13 produced only one peak (Fig 1D). These observations led us to suspect that oxidized NCR13 was expressed in our *P. pastoris* expression system as two species differing in length or disulfide cross-linking pattern. Mass spectrometry analysis of peptides purified from both HPLC peaks revealed identical molecular weights (S1 Fig) as expected for NCR13 with three disulfide bonds, narrowing our suspicion to different disulfide bonding patterns. Across various batches of purified NCR13, peak 1 was consistently observed to contain less peptide than peak 2 (S1 Table). Peak 1 and peak 2 peptides are hereafter referred to as NCR13_peptide folding variant 1 (NCR13_PFV1) and NCR13_PFV2 respectively.

A

```
CaNCR13  -TKPCQSDKDCKKFACRKPKVPKCINGFCKCVR-  32
CaNCR15  TKQPCKSRKHCKTYRCPTPKVPNCVNGFCKCVR-  33
CaNCR07  KKMPCKRRRDCKTYPCPHPKVRDCVKGYCKCVVR  34
```

B

Peptide	Net Charge	% Hydrophobic amino acids	Predicted MW (kDa)	Isoelectric point	% identity with NCR13
CaNCR13	+8	28.1	3.66	9.59	100
CaNCR15	+9	24.2	3.81	9.82	66.6
CaNCR07	+10	26.5	4.08	9.85	48.4

C

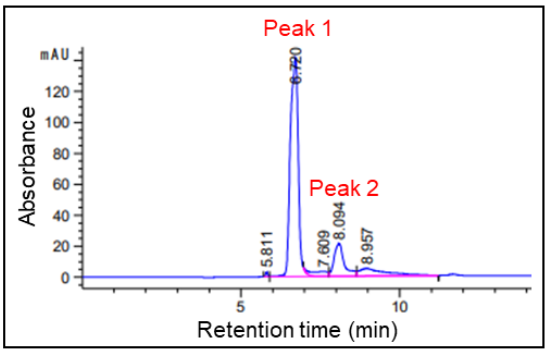

D

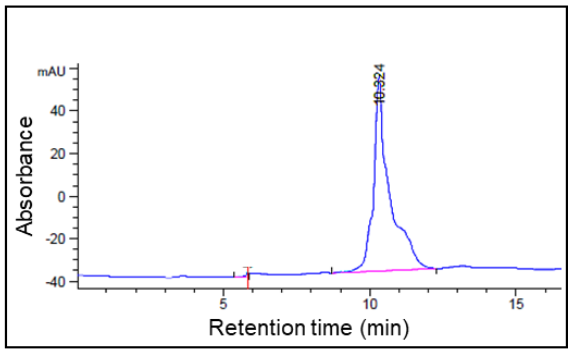

Fig 1. Primary amino acid sequence and properties of NCR13. (A) Primary amino acid sequences for Chickpea (*C. arientinum*) NCR13 and its homologs NCR15 and NCR07. Conserved cysteine residues are highlighted in red. The number of amino acids is indicated at the end of each sequence. (B) Peptide characteristics of CaNCR13, CaNCR15 and CaNCR07. (C) High-performance liquid chromatography (HPLC) analyses of NCR13 produced recombinantly in *Pichia pastoris*, monitored at 260 nm, reveals the presence of two major products. mAU represents milli-Absorbing Units. (D) Chemically synthesized NCR13 elutes as one HPLC peak.

To further characterize both NCR13_PFVs, we performed NMR structural analysis of ^{15}N-labeled NCR13_PFV1 and NCR13_PFV2. Fig 2A and B show the assigned ^{1}H-^{15}N HSQC spectra for NCR13_PFV1 and NCR13_PFV2, respectively. The broad dispersion of amide chemical shifts in both spectral dimensions is a standard feature of a structured peptide (25). As illustrated in Fig 2, assignment of both spectra was consistent with the primary amino acid sequence of NCR13.

173 However, the pattern of the fingerprint ^{1}H-^{15}N HSQC spectrum for both peptides was clearly
174 different, suggesting their structures were unique. Given that the primary amino acid sequence of
175 NCR13 contains six cysteine residues (C4, C10, C15, C23, C28, and C30) that can form fifteen
176 different patterns of intramolecular disulfide bonds when all six are oxidized, our attention
177 immediately focused on a different disulfide bond pattern for the two peptides. Treatment of both
178 peptides with the reducing agents dithiothreitol (DTT) or tris(2-carboxyethyl) phosphine resulted
179 in the identical ^{1}H-^{15}N HSQC spectrum shown in Fig 2C, illustrating that the parent primary amino
180 sequence was identical for both peptides. Note that when the NCR13 cysteines are all in the
181 reduced (dithiol) state, dispersion of amide chemical shifts in both spectral dimensions were
182 distinctively narrow, a standard feature of an unstructured protein (25, 26). As observed for *M.*
183 *truncatula* NCR044 (19), disulfide bond formation is essential to stabilize the elements of
184 secondary structure observed in the oxidized state because in the reduced state the peptide is
185 largely disordered.

186 Disulfide bond formation between all six cysteine residues in NCR13_PFV1 and
187 NCR13_PFV2 was unambiguously verified from the NMR chemical shifts of the cysteine side
188 chain β-carbon. In general, the cysteine $^{13}C^{\beta}$ chemical shift is greater than 35 ppm in the oxidized
189 state and under 32 ppm in the reduced state. As summarized in S2 Table, the $^{13}C^{\beta}$ chemical shift
190 for all six cysteines in both isoforms of oxidized NCR13 are between 37 and 48 ppm, indicating
191 they are all oxidized in NCR13_PFV1 and NCR13_PFV2. Due to the number of potential disulfide
192 bond patterns that the six cysteine residues can adopt, it was not possible to use NMR structures
193 in early calculations to unambiguously deduce disulfide bond pairs from ^{1}H-^{1}H NOEs that arise
194 due to proximal γ-sulphur atoms in the disulfide state. Instead, as previously applied to NCR044,
195 the disulfide bond pattern was inferred from the analysis of mass spectral data for trypsin-digested,

unlabeled protein in the oxidized and reduced states (19). For NCR13_PFV2, this approach showed that the disulfide bonds were C4-C10, C15-C30, and C23-C28 (S2 Fig). For NCR13_PFV1, despite extensive modification of the experimental procedures, this approach failed due to the hyperstability of this isoform towards trypsinization. Consequently, the disulfide bond pattern predicted by AlphaFold (27) C4-C23, C10-C28, and C15-C30 was used to calculate the ensemble of NMR structures for NCR13_PFV1. The two NCR13 isoforms share one identical disulfide bond, C15-C30, and S2 Table shows that these cysteine $^{13}C^{\beta}$ chemical shifts differ less than 0.5 ppm, strongly suggesting this disulfide bond is present in both isoforms. As will be discussed below, this disulfide bond pattern best supports the experimental NOE data.

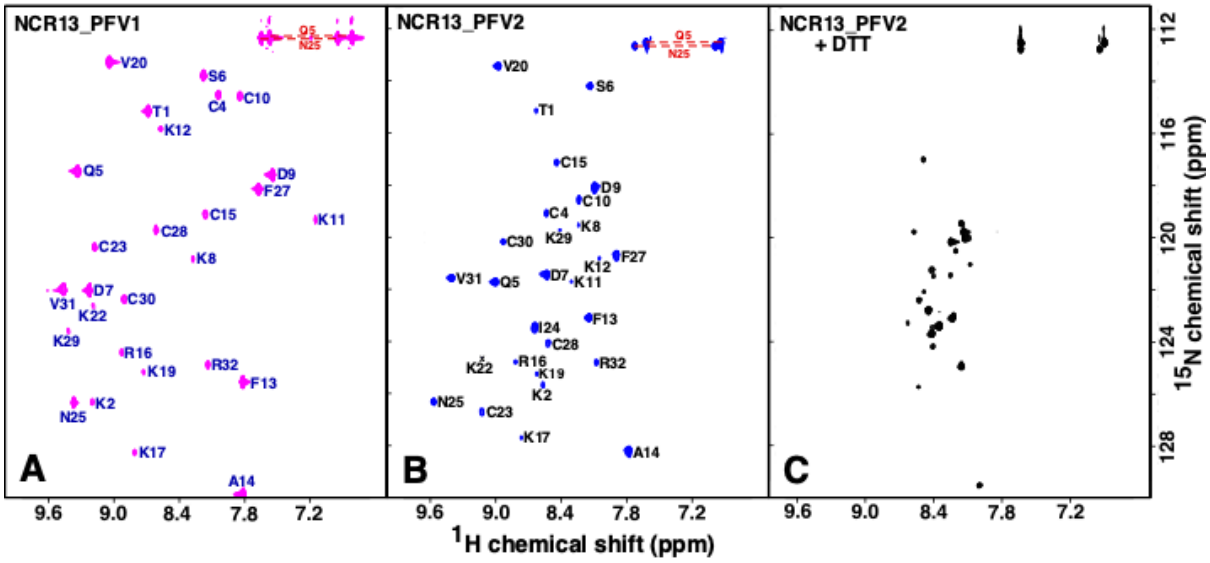

Fig 2. Fingerprint ^{1}H-^{15}N HSQC spectra for oxidized and reduced NCR13. Assigned ^{1}H-^{15}N HSQC spectra for oxidized (disulfide) NCR13_PFV1 (A) and NCR13_PFV2 (B). (C) The ^{1}H-^{15}N HSQC spectrum of fully reduced (dithiol) NCR13_PFV1 and NCR13_PFV2 were identical (the spectrum for NCR13_PFV2 is illustrated). All spectra collected on ~ 1 mM samples at 20°C in 20 mM sodium acetate, 50 mM NaCl, pH 5.3 at a ^{1}H resonance frequency of 600 MHz. Amide side chain resonance pairs are connected by a red dashed line. Not within the displayed spectral boundaries is the G26 amide resonance for NCR13_PFV1 and NCR13_PFV2 at 8.66/103.1 ppm and 7.99/101.7 ppm, respectively, and the I24 amide resonance for NCR13_PFV1 at 8.72/132.0 ppm.

Three-dimensional NMR solution structures of NCR13_PFV1 and NCR13_PFV2

To obtain structural insights into NCR13_PFVs, we performed NMR analyses of the oxidized forms of these two peptides. Fig 3 illustrates a superposition of cartoon representations of the final ensemble of structures calculated for the two NCR13 PFVs (left) with the main chain of a single structure shown to the right of the ensemble with the disulfide bonds highlighted in different colors. The elements of secondary structure are essentially identical in both isoforms, one anti-parallel β-sheet (V20-I24, F27-V31) and a short a-helix (Q5 or S6–C10). However, the disulfide bond pattern markedly alters the relative orientation of these elements of secondary structure. Both peptides contain one identical disulfide bond, C15-C30, that ties the N-terminal end of the peptide to approximately the middle of the linker region between the two elements of secondary structure. The consequence is that in NCR13_PFV1 the α-helix sits over the top of the face of the β-sheet while in NCR13_PFV2 the α-helix sits on the side of the β-sheet. This difference is better illustrated in S3 Fig, a cartoon illustration of two representative structures superimposed on the β-strand. This results in a smaller accessible surface area for NCR13_PFV1 (3188 ± 63 $Å^2$) than for NCR13_PFV2 (3357 ± 129 $Å^2$). The more compact structure for NCR13_PFV1, with the disulfide bonds formed between C4, C10, C23, and C28 directed into the interior of the peptide, may protect these disulfide bonds from reduction and contribute to the hyperstability of NCR13_PFV1 towards reduction. Disulfide bonds may also be protected from reduction because this NCR13 isomer is less dynamic. This suggestion is indirectly made by comparing the ensemble of calculated solution structures illustrated in Fig 3. The ensemble of structures calculated for NCR13_PFV1 converge to a greater extent than for NCR13_PFV2 with the backbone (N-C^a-C=O) RMSD to the mean for the ordered residues almost twice as large for NCR13_PFV2 (0.41 ± 13 Å versus 0.76 ± 20 Å, respectively; S3 Table). While this difference reflects the greater number of NOEs observed for

239 NCR13_PFV1 (316) than for NCR13_PFV2 (119) (S3 Table) due to a more compact structure, it
240 also indirectly suggests the NCR13_PFV1 explores less conformational space than NCR13_PFV2.
241 To further verify that the AlphaFold predicted disulfide bond pattern was correct for
242 NCR13_PFV1, an NMR structure was calculated using only the NOE and TALOS+ (dihedral
243 angle) data (no hydrogen bonds) with the other possible disulfide bond pattern (C4-C28, C10-C23,
244 and C15-C30). In S4A Fig, two representative cartoon structures that result from the two possible
245 disulfide bond patterns are superimposed on the β-strands. In the reversed, C4-C28/C10-C23
246 disulfide pattern (yellow), the direction of α1 is also reversed relative to the β-strand and this
247 prevents the N-terminal region (T1-P3) from making close contact with the β-strand. While most
248 of the NOEs were satisfied in both structure calculations, long range experimental NOEs between
249 the N-terminal region of NCR13_PFV1 (T1-P3) and the β-strand were only satisfied with the C4-
250 C23/C10-C28 disulfide pattern used in the structure deposited to the PDB (8UTM), suggesting
251 this pattern was correct. Furthermore, as shown in S4B Fig, the predicted AlphaFold structure for
252 NCR13_PFV1 was like the experimental structure (8UTM). In both structures, the β-sheet is
253 almost identical with the major difference a slightly shorter α-helix displaced two residues (D7-
254 K11 versus Q5-C10 experimentally) that packs against the β-strand a bit differently in the
255 AlphaFold structure (green). Most relatively, the N-terminal region (T1-P3) folds towards the β-
256 strand in the AlphaFold predicted structure, as verified experimentally with the long-range NOEs
257 between these regions.
258
259

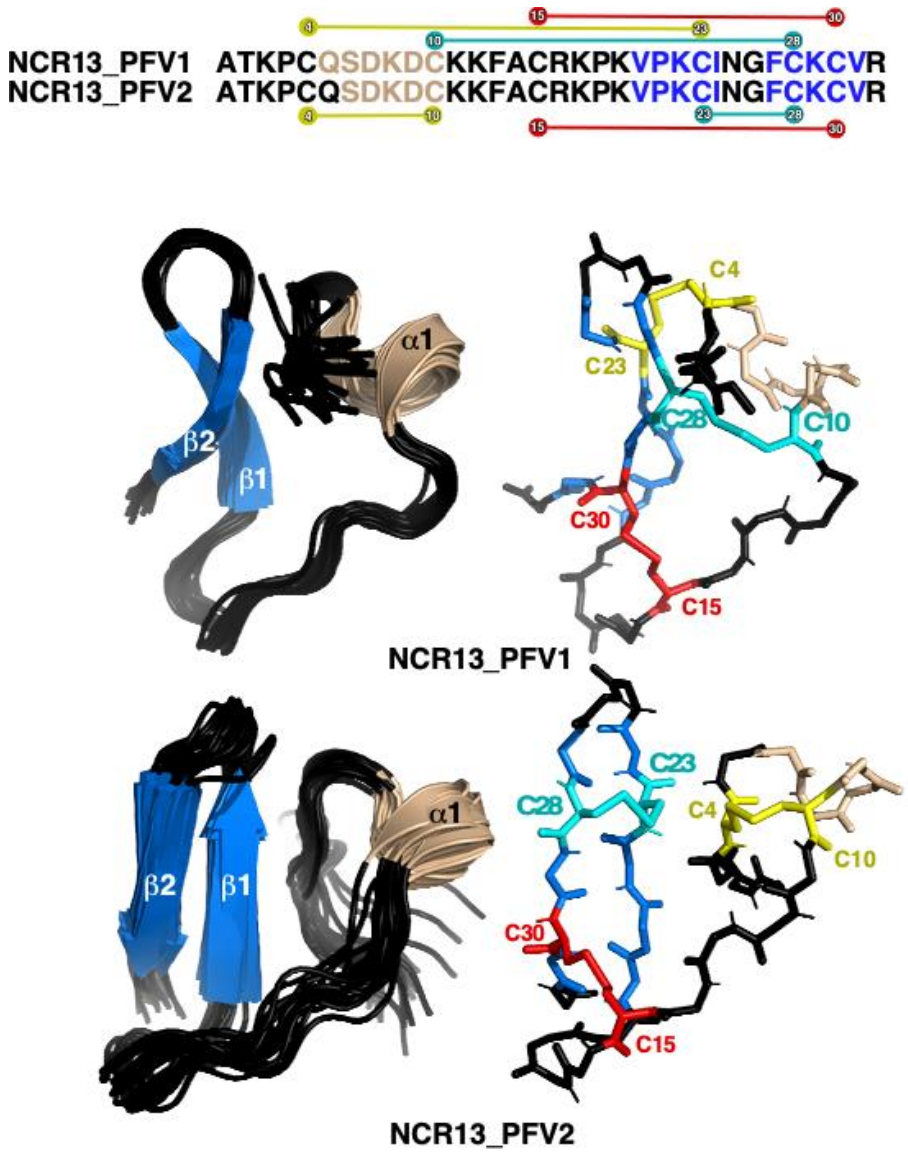

Fig 3. Three-Dimensional NMR solution structure of NCR13_PFV1 and NCR13_PFV2. Cartoon representation of the backbone superposition of the ordered regions in the ensemble of 20 structures calculated for oxidized NCR13_PFV1 (8ULM) and NCR13_PFV2 (7TH8). β-strands are colored blue and labeled sequentially starting from the N-terminal and the lone α-helix is colored wheat. Next to each ensemble is a backbone stick representation of a single structure with the six oxidized cysteine side chains highlighted in yellow, red, or cyan. Above the structures is a schematic summary of the elements of secondary structure observed for the two NMR structures, color-coded similarly. Also shown in the schematic are the disulfide bond connections in both isomers. One disulfide bond, between C15 and C30 (red), is identical in both isomers with C10 and C28 swapping disulfide bond partners.

NCR13_PFV1 exhibits much greater antifungal activity against fungal pathogens than NCR13_PFV2

Having found striking differences in their NMR structures, we investigated the *in vitro* antifungal activity of NCR13_PFV1 and NCR13_PFV2 against three necrotrophic plant fungal pathogens (19). NCR13_PFV1 inhibited the growth of *B. cinerea* at the Minimal Inhibitory Concentration (MIC) of 0.09 µM. Conversely, NCR13_PFV2 inhibited *B. cinerea* at the MIC of 1.5 µM (Figs 4A-C), seventeen-fold higher than that of NCR13_PFV1. Chemically synthesized NCR13 had a MIC of 3 µM, two-fold higher than NCR13_PFV2 (Fig 4B), suggesting that this fully reduced synthesized product was yet another isoform of NCR13 and illustrating the importance of disulfide bonds for antifungal activity. Similarly, NCR13_PFV1 showed several fold greater antifungal activity against *Fusarium virguliforme,* and *Sclerotinia sclerotiorum* compared to NCR13_PFV2 (Fig 4A). Overall, these results reveal that NCR13_PFV1 is a much more potent antifungal peptide compared to NCR13_PFV2.

A

Pathogen	NCR13_PFV1	NCR13_PFV2
	MIC (µM)	
Botrytis cinerea	0.09	1.5
Fusarium virguliforme	0.09	1.5
Sclerotinia sclerotiorum	6.0	24

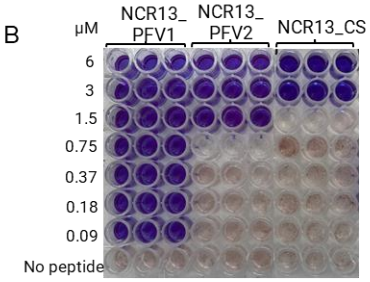

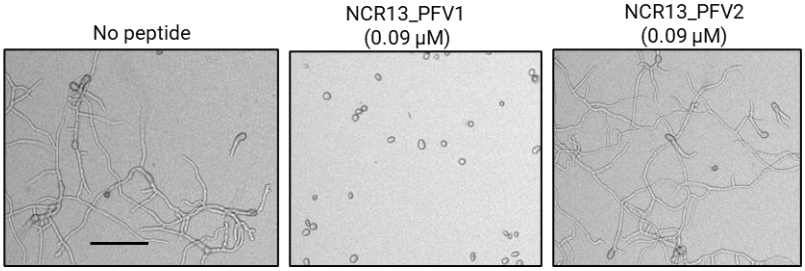

Fig 4. NCR13_PFV1 exhibits potent antifungal activity compared to NCR13_PFV2. (A) Minimal Inhibitory Concentration (MIC) values of NCR13_PFVs for different fungal pathogens. (B) Antifungal activity of NCR13_PFV1, NCR13_PFV2, and chemically synthesized NCR13 (NCR13_CS) against *B. cinerea*. Fungal cell viability assay using resazurin dye. Change from blue

290 to pink/colorless signals resazurin reduction and indicates metabolically active *B. cinerea*
291 germlings after 60 h. NCR13_PFVs are used at concentrations of 0.09 - 6 µM. NCR13_PFV1 at a
292 concentration 0.045 µM had no antifungal activity (data not shown). N = 3, N indicates biological
293 replicates. (C) Representative microscopic images showing the inhibition of *B. cinerea* growth 24
294 h after treatment with 0.09 µM NCR13_PFVs (Right). *B. cinerea* without peptide added served as
295 a negative control (Left). Scale bar = 100 µm.
296
297 **Disulfide bonds in NCR13_PFV1 contribute to the antifungal activity and formation of**
298 **peptide folding variants**
299 Fully oxidized NCR13_PFV1 contains three disulfide bonds: C4-C23, C10-C28, and C15-C30.
300 The potent antifungal activity of NCR13_PFV1 against *B. cinerea* at nanomolar concentrations
301 prompted us to investigate the contribution of each disulfide bond towards antifungal activity and
302 the formation of folded variants when expressed in *P. pastoris*. We carried out functional analysis
303 of these disulfide bonds by creating three dual Cys to Ser variants to systematically remove one
304 disulfide bond: NCR13_C4S-C23S, NCR13_C10S-C28S, and NCR13_C15S-C30S variants (Fig
305 5A). These knockout variants were expressed in *P. pastoris* and purified. HPLC profiles of
306 NCR13_C4S-C23S, and NCR13_C15S-C30S revealed a single peak whereas NCR13_C10S-
307 C28S revealed two peaks (Fig 5B), the latter observation suggesting NCR13_C10S-C28S folded
308 with at least two different disulfide bonding patterns. Mass spectrometry analysis confirmed the
309 expected molecular mass of each peptide (S4 Table), consistent with them being in an oxidized
310 state. Therefore, our results indicate that the disulfide pairing of C4-C23 and C15-C30 is essential
311 for the formation of NCR13_PFVs.
312 All three single disulfide bond knockouts had lower antifungal activity against *B. cinerea*
313 compared to NCR13_PFV1, as summarized in Fig 5. NCR13_C4S-C23S and NCR13_C15S-
314 C30S both inhibited *B. cinerea* with a MIC value of 1.5 and 0.75 µM respectively, while the
315 products in the two NCR13_C10S-C28S HPLC peaks had a MIC of 3 µM (Fig 5C and D). While

316 we were unable to confirm the disulfide bonding pattern in each of these knockout variants, the
317 MIC data indicates that each disulfide bond contributes to the antifungal activity of NCR13_PFV1
318 (Fig 5C and D). Indeed, a NCR13 construct with all six Cys residues replaced with Ser (NSR13)
319 was inactive against *B. cinerea* even at the highest tested concentration, 24 µM (Fig 5C and D, S4
320 Fig). It is likely that NSR13 is unfolded, as suggested by the NMR data for reduced NCR13 (Fig
321 2) and its late elution time on a reverse phase column. Therefore, it may be concluded that each
322 disulfide bond contributes to the antifungal activity of the NCR13.

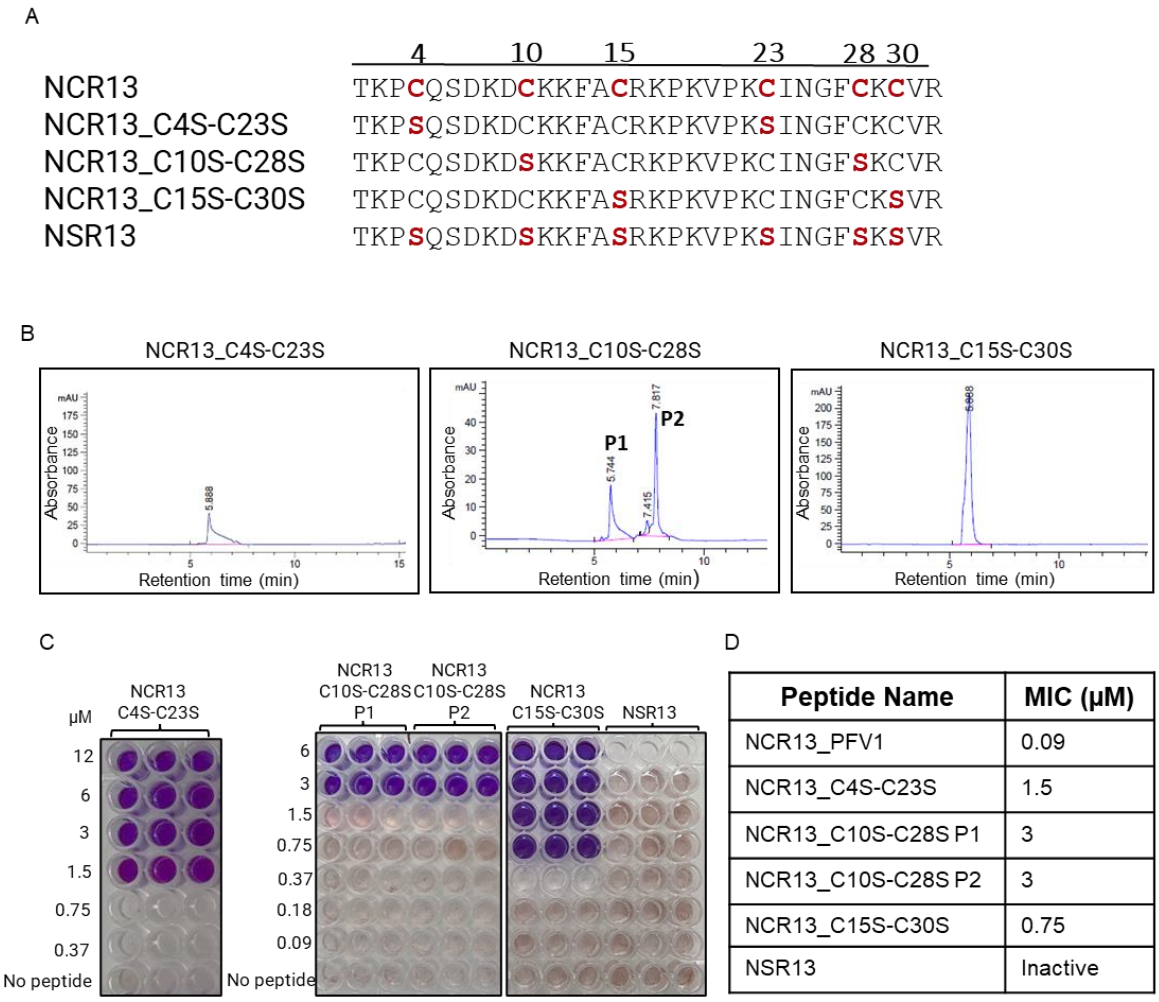

Peptide Name	MIC (µM)
NCR13_PFV1	0.09
NCR13_C4S-C23S	1.5
NCR13_C10S-C28S P1	3
NCR13_C10S-C28S P2	3
NCR13_C15S-C30S	0.75
NSR13	Inactive

323

324 **Fig 5. Removing disulfide bonds in NCR13_PFV1 strongly reduces antifungal activity**
325 **against *B. cinerea in vitro*.** (A) Four NCR13 constructs are used to assay the importance of
326 disulfide bond formation for antifungal activity by substituting pairs of Cys residues with Ser
327 (highlighted in red). The numbers above the sequence indicate the position of the Cys substitution.

328 (B) HPLC analyses of NCR13_C4S-C23S, NCR13_C10S-C28S, and NCR13_C15S-C30S
329 recombinantly produced in *P. pastoris* monitored at 260 nm (mAU = milli-Absorbing Units). (C)
330 Fungal cell viability assay of disulfide knockout variants. A color change from blue to pink/clear
331 indicative of metabolically active (live) *B. cinerea* germlings after 60 h. (D) Summary of the MIC
332 values for NCR13_PFV1 and NCR13 disulfide knockout variants.
333

334 **Identification of the sequence motif governing the antifungal activity of NCR13**

335 To identify the sequence motif governing the antifungal activity of NCR13 against *B. cinerea*, we
336 purchased chemically synthesized alanine scanning variants NCR13_AlaV1 through
337 NCR13_Ala5 (Fig 6A). These variants contained a string of three to five consecutive Alanine (Ala)
338 residues substituted throughout the NCR13 sequence. We then compared their antifungal activity
339 relative to a chemically synthesized NCR13. Notably, our findings revealed that NCR13_AlaV2,
340 NCR13_AlaV3, and NCR13_AlaV4 had no antifungal activity against *B. cinerea* at the highest
341 tested concentration, 12 μM (Fig 6A, S6A Fig), whereas NCR13 inhibited this pathogen at an MIC
342 of 3 μM. This data suggested that a 13-residue, Lys-rich motif, KKFA**C**RKPKVPK**C,** located in
343 the random coil and β-strand region, was a major determinant of NCR13 antifungal activity. We
344 further explored the importance of this motif by testing antifungal activity of NCR13_AlaV3
345 expressed in *P. pastoris* to allow formation of disulfide bonds and found that it also lacked
346 antifungal activity against *B. cinerea* like the chemically synthesized NCR13_AlaV3 (S6B Fig). It
347 is noteworthy that NCR13_AlaV1 and NCR13_AlaV5 also displayed 2- and 4-fold reduction,
348 respectively, in the antifungal activity against *B. cinerea* indicating that the N-terminal QSDKD
349 and C-terminal INGF motifs are relatively minor contributors to the antifungal activity of this
350 peptide. (Fig 6A).
351

A

Peptide	Sequence	MIC (μM)
NCR13_CS	TKPCQSDKDCKKFACRKPKVPKCINGFCKCVR	3
NCR13_AlaV1	TKPC**AAAAA**CKKFACRKPKVPKCINGFCKCVR	6
NCR13_AlaV2	TKPCQSDKDC**AAAA**CRKPKVPKCINGFCKCVR	Inactive (>12)
NCR13_AlaV3	TKPCQSDKDCKKFAC**AAAA**VPKCINGFCKCVR	Inactive (>12)
NCR13_AlaV4	TKPCQSDKDCKKFACRKPK**AAA**CINGFCKCVR	Inactive (>12)
NCR13_AlaV5	TKPCQSDKDCKKFACRKPKVPKC**AAAA**CKCVR	12

B

Fig 6. Active motif of NCR13 required for antifungal activity. (A) Antifungal activity of NCR13 synthetic peptide and NCR13 alanine variants against *B. cinerea*. Alanine scanning mutagenesis was done by substituting alanine within the NCR13 core sequence, leading to the creation of the NCR13_AlaV1-V5. MIC values were determined against *B. cinerea*. The amino acid substitutions are shown in red. Representative pictures are shown in S5 Fig. (B) Active motif of NCR13 (highlighted with a bold red font) required for its antifungal activity against *B. cinerea.* The secondary structure elements are shown above the amino acid sequence. The gray line and green arrow indicate α-helix (α1) and β-strand (β1) respectively.

NCR13_PFV1 disrupts the plasma membrane of *B. cinerea* faster than NCR13_PFV2

Since NCR13_PFV1 exhibits ~17-fold more potent antifungal activity against *B. cinerea* than NCR13_PFV2, we hypothesized that the difference in antifungal activity lies in differential membrane permeabilization ability. To test this hypothesis, we performed SYTOX™ Green (SG) assays to examine the ability of NCR13_PFV1 and NCR13_PFV2 at 0.09 μM to permeabilize the plasma membrane of *B. cinerea* germlings. SG, a membrane-impermeant dye, binds to nucleic

368 acids and is an indicator of membrane permeability. Average fluorescence intensities were
369 measured along different time points and NCR13_PFV1 showed much higher fluorescence
370 intensity within exposed cells than NCR13_PFV2 (Fig 7A and B). After 10 min, SG uptake was
371 observed in germlings challenged with NCR13_PFV1 but not in germlings challenged with
372 NCR13_PFV2. After 20 min, a very strong SG uptake signal was observed in NCR13_PFV1
373 treated germlings, but only a modest signal in NCR13_PFV2 treated germlings (Fig 7A and B).
374 Thus, NCR13_PFV1 inhibited fungal growth to a greater degree than NCR13_PFV2 at nanomolar
375 concentration in part by permeabilizing the plasma membrane of *B. cinerea*.
376

377 **NCR13_PFV1 and NCR13_PFV2 reveal quantitative differences in their binding to multiple**
378 **membrane phospholipids**

379 Antifungal plant defensins gain entry into fungal cells and bind to a variety of bioactive
380 phospholipids resident on the plasma membrane (9). We speculated that NCR13_PFV1 and
381 NCR13_PFV2 differ in their phospholipid binding specificity in the context of membrane bilayer.
382 Therefore, we used phospholipid strip assays to determine if NCR13_PFVs bind to different
383 phospholipids. Our findings revealed that both NCR13_PFV1 and NCR13_PFV2 interacted with
384 several phospholipids, including phosphatidylinositol 4-phosphate [PI(4)P] and PI(4,5)P_2 (Fig
385 7C). NCR13_PFV2 displayed significantly stronger binding affinity to phosphoinositides such as
386 PI(3)P, PI(4)P, PI(5)P, PI(4,5)P_2, and PI(3,4,5)P_3 than NCR13_PFV1 (Fig 7D). The interaction of
387 PI(4)P and PI(4,5)P_2 with NCR13_PFV1 and NCR13_PFV2 were further validated using a
388 polyPIPosome binding assay (Fig 7E). Nevertheless, the significance of the phospholipid binding
389 differences between the two peptides for their antifungal activity requires further investigation.
390 Since several antifungal plant defensins bind to membrane phospholipids to oligomerize and

391 induce membrane permeabilization (28), we tested the ability of NCR13_PFV1 and NCR13_PFV2
392 to oligomerize by incubating the peptides with the biochemical cross-linker
393 bis(sulfosuccinimidyl)suberate (BS_3) in the presence and absence of PI(4,5)P_2. NCR13_PFV1
394 formed oligomers both in the presence and absence of PI(4,5)P2. On the other hand, NCR13_PFV2
395 formed higher order oligomers, but, only at higher concentrations (115 µM and 330 µM) of
396 PI(4,5)P_2 (S7 Fig). Therefore, further investigation is required to determine whether phospholipid
397 binding, including PI(4,5)P2, and the oligomerization of NCR13_PFVs are critical for antifungal
398 activity.

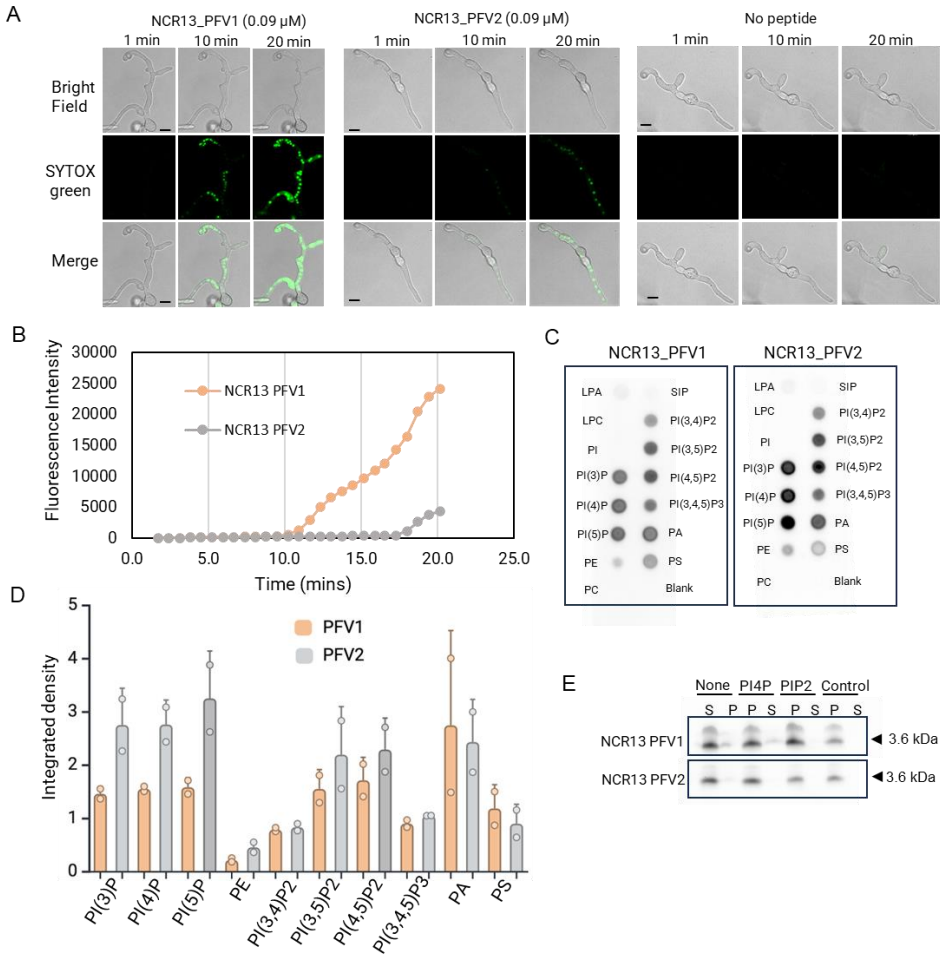

399

400 **Fig 7. NCR13 PFV1 permeabilizes the cell membrane of *B. cinerea* rapidly.** (A) Confocal
401 microscopy images of SYTOX Green (SG) uptake in *B. cinerea* germlings at different time points.

402 Germlings were treated with 0.09 μM NCR13_PFVs and SG dye simultaneously for 20 min. No
403 peptide is used as a control. Scale bars = 10 μm. The experiment was repeated thrice with similar
404 results. (B) Quantitative measurements of average fluorescence intensity over time to assess cell
405 membrane permeability in *B. cinerea* germlings treated with 0.09 μM NCR13 PFVs. (C) PIP strip
406 showing binding of NCR13 PFVs to multiple phospholipids, including phosphatidylinositol 4,5-
407 bisphosphate (PI(4,5)P_2), phosphatidylinositol (3,4,5)-trisphosphate PI(3,4,5)P_3 and
408 phosphatidylinositol monophosphates PI(3)P, PI(4)P, and PI(5)P, phosphatidylinositol
409 bisphosphate PI(3,4)P_2. (D) Integrated density measurement of PIP strip probed with
410 NCR13_PFVs. Datapoints are means ± SE of two independent biological replicates ($N = 2$). (E)
411 Binding of NCR13_PFVs to PI(4)P and PI(4,5)P2 (PIP_2) containing liposomes. NCR13_PFV's
412 were incubated without liposomes (None) and liposomes bearing no phosphoinositides (control),
413 S- supernatant fraction and P- pellet fraction.
414

415 **NCR13 PFV1 is internalized faster in germling cells of *B. cinerea* than NCR13_PFV2**

416 Due to its much greater antifungal activity *in vitro* against *B. cinerea*, we hypothesized that
417 NCR13_PFV1 exhibited faster entry into fungal cells at its MIC than NCR13_PFV2. To test this
418 hypothesis, we exposed *B. cinerea* germlings to 0.09 μM DyLight550-labeled NCR13_PFV1 and
419 NCR13_PFV2 and monitored their entry into germlings of *B. cinerea* using confocal microscopy.
420 Within ~30 min, NCR13_PFV1 penetrated the germlings; however, NCR13_PFV2 did not enter
421 the germlings (Fig 8A and B). At a concentration of 1.5 μM, NCR13_PFV1 started entering
422 germlings in ~4 min, while NCR13_PFV2, after briefly gathering on the cell surface (Fig 8C,
423 white arrowheads), started entering germlings at ~8 min. Unlike NCR13_PFV2's lack of entry at
424 0.09 μM, delayed entry of NCR13_PFV2 was evident at 1.5 μM (Fig 8C and D).

425 Following entry into *B. cinerea* germling cells, both NCR13_PFV1 and NCR13_PFV2
426 accumulated in distinct subcellular foci (Fig 8E, white arrows). Further localization studies using
427 the nuclear staining dye Hoechst 33258 revealed that both peptides were localized in the nuclei.

428 To determine if each peptide was sub-localized within the nucleolus, we used the nucleolus-
429 specific RNA staining dye Nucleolus Bright Green. As shown in Fig 8F, each peptide was localized
430 within the nucleolus of germling cells suggesting that each peptide likely binds to ribosomal RNA
431 (rRNA) or proteins and interferes with protein synthesis.

432 To gain further insight into the MoA of NCR13_PFV1 and NCR13_PFV2, we assessed the
433 stability of each peptide once inside *B. cinerea* cells. We challenged *B. cinerea* germlings with
434 each peptide separately for two different time points, 2 h and 4 h, and tested the stability of each
435 peptide in fungal cells through western blot analysis. An NCR13 polyclonal antibody capable of
436 binding to each peptide with equal affinity was used for this analysis (S8 Fig). NCR13_PFV1
437 accumulated in germling cells within 2 h and accumulates further after 4 h. In contrast, much less
438 NCR13_PFV2 accumulated in germling cells within 2 h and was strongly decreased by 4 h (Fig
439 8E). Therefore, we highlight NCR13_PFV1 more rapidly enters fungal cells than NCR13_PFV2,
440 and once inside NCR13_PFV1 is likely more stable than NCR13_PFV2.

441

442

443

444

445

446

447

448

449

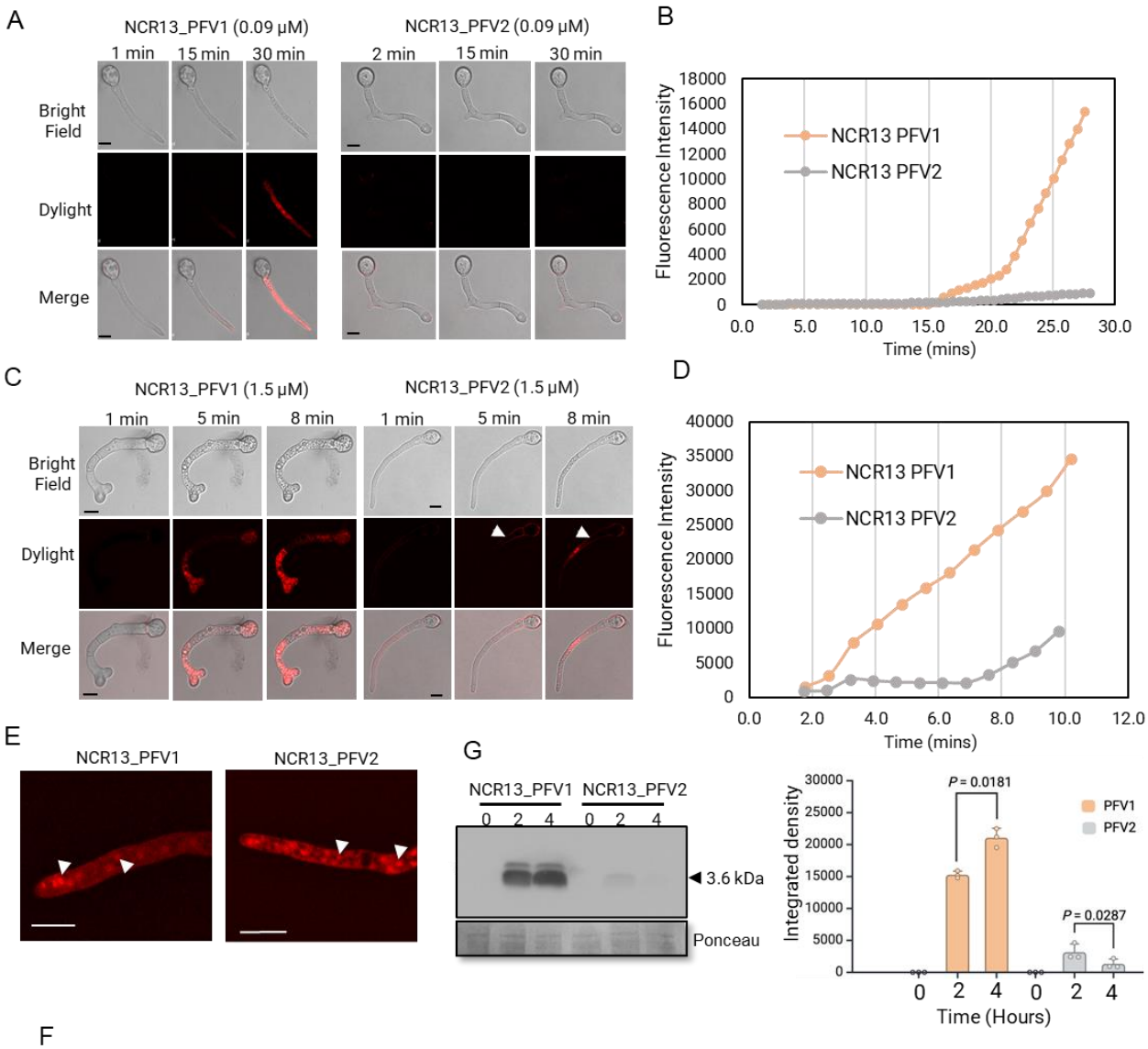
A
NCR13_PFV1 (0.09 μM)
1 min
15 min
30 min
NCR13_PFV2 (0.09 μM)
2 min
15 min
30 min
Bright Field
Dylight
Merge
B
Fluorescence Intensity
NCR13 PFV1
NCR13 PFV2
Time (mins)
C
NCR13_PFV1 (1.5 μM)
1 min
5 min
8 min
NCR13_PFV2 (1.5 μM)
1 min
5 min
8 min
Bright Field
Dylight
Merge
D
Fluorescence Intensity
NCR13 PFV1
NCR13 PFV2
Time (mins)
E
NCR13_PFV1
NCR13_PFV2
G
NCR13_PFV1
NCR13_PFV2
0 2 4 0 2 4
3.6 kDa
Ponceau
Integrated density
P = 0.0181
P = 0.0287
PFV1
PFV2
Time (Hours)

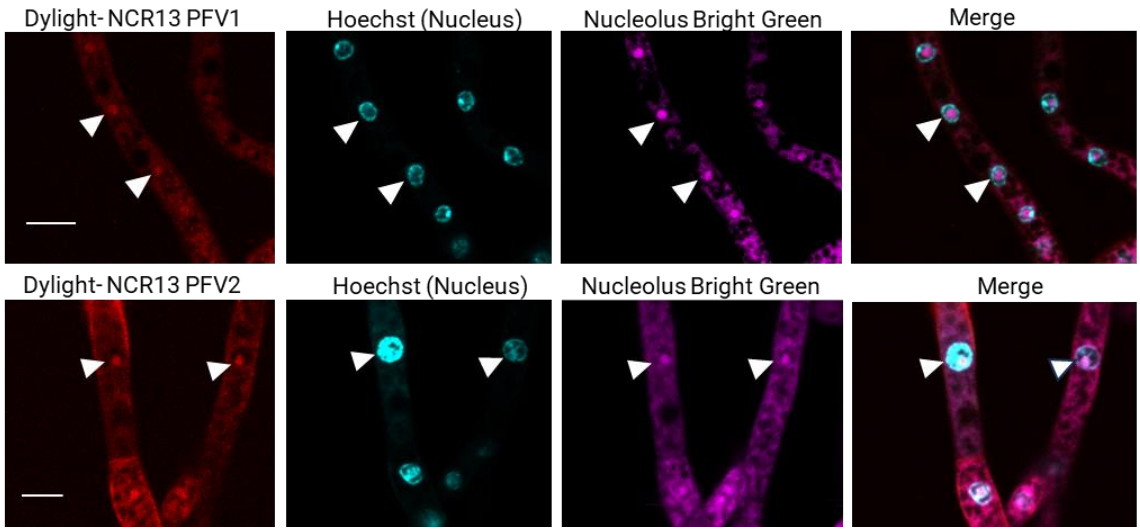
F
Dylight- NCR13 PFV1
Hoechst (Nucleus)
Nucleolus Bright Green
Merge
Dylight- NCR13 PFV2
Hoechst (Nucleus)
Nucleolus Bright Green
Merge

450

451 **Fig 8. Internalization and localization of NCR13 PFVs in *B. cinerea* germlings.** (A) Confocal
452 microscopy images of *B. cinerea* germlings at different points treated with 0.09 μM DyLight550-
453 labeled NCR13_PFV1 (left) and NCR_PFV2 (right) for 30 minutes. Scale bars = 10 μm. Data
454 represents representative results of three independent experiments. (B) Quantification of peptide
455 internalization was conducted by analyzing the average fluorescence intensities over time (in
456 minutes) for NCR13_PFVs. The upper threshold for background was set at 23 for Fiji analysis.
457 (C) Confocal microscopy images of *B. cinerea* germlings treated with 1.5 μM DyLight550-labeled
458 NCR13_PFVs for 30 minutes. White arrowheads indicate NCR13_PFV2 on the cell surface. Scale
459 bars = 10 μm. (D) Quantitative measurements of peptide internalization in *B. cinerea* germlings
460 treated with 1.5 μM NCR13_PFV1 (left) and NCR13_PFV2 (right). (E) Internalized DyLight550-
461 labeled NCR13_PFV1 (left) and NCR13_PFV2 (right) concentrate in specific foci (white
462 arrowheads) within *B. cinerea* germlings. Scale bars = 10 μm. (F) NCR13_PFV1 and
463 NCR13_PFV2 localize to the nucleolus. DyLight550-labeled NCR13_PFV1 (upper panel) and
464 PFV2 (lower panel) colocalize with rRNA-specific Nucleolus Bright Green stain. Hoechst 33258
465 is used for staining nucleus. White arrowheads indicate nucleolar localization. Scale bars = 5 μm.
466 (G) Semi-quantitative analysis of NCR13_PFVs within *B. cinerea* germlings. Germlings were
467 treated with 1.5 μM NCR13_PFV1 and NCR13_PFV2 for 0, 2, and 4 hours. Total proteins were
468 extracted from fungal cells and immunoblotted using anti-NCR13 antibody. Equal loading of
469 proteins was verified using Ponceau staining. The bar graph represents integrated density
470 measurements. Statistical significance was tested using paired student's t-test. Data are shown as
471 mean ± SD (N = 3, where N refers to biological replicates).

472

473 **NCR13_PFV1 binds to rRNA and is a more potent inhibitor of protein translation *in vitro***
474 **than NCR13_PFV2**

475 Since NCR13_PFVs are localized in the nucleoli of *B. cinerea*, we decided to test the binding of
476 each peptide to rRNA. This was accomplished with an Electrophoretic Mobility Shift Assay
477 (EMSA) (29) by incubating each peptide with total rRNA isolated from *B. cinerea* germlings. Our
478 results showed that NCR13_PFV1 retarded the mobility of the rRNA at all concentrations greater
479 than 0.18 μM, while NCR13_PFV2 showed no binding to rRNA until 3 μM (Fig 9A, S8 Fig).
480 Therefore, it is evident that NCR13_PFV1 exhibits stronger binding affinity to fungal rRNA than
481 NCR13_PFV2.

482 Next, we tested the ability of the NCR13_PFVs to inhibit protein translation *in vitro* because we
483 hypothesized that NCR13_PFV1 may be a more potent inhibitor of protein translation than
484 NCR13_PFV2. This was accomplished using a wheat germ *in vitro* translation system based on a
485 luciferase activity (30). Protein translation inhibitory activity of each peptide was concentration
486 dependent (Fig 9B). NCR13_PFV1 inhibited translation more effectively than NCR13_PFV2 at
487 concentrations more than 0.75 µM. At 24 µM, NCR13_PFV1 almost completely halted translation
488 compared to the ~50% inhibition by NCR13_PFV2 (Fig 9B). Based on these results, the difference
489 in the antifungal potency of NCR13_PFVs may be partly due to the inhibition of protein translation
490 *in vivo* with NCR13_PFV1 being a more potent protein translation inhibitor in *B. cinerea*.

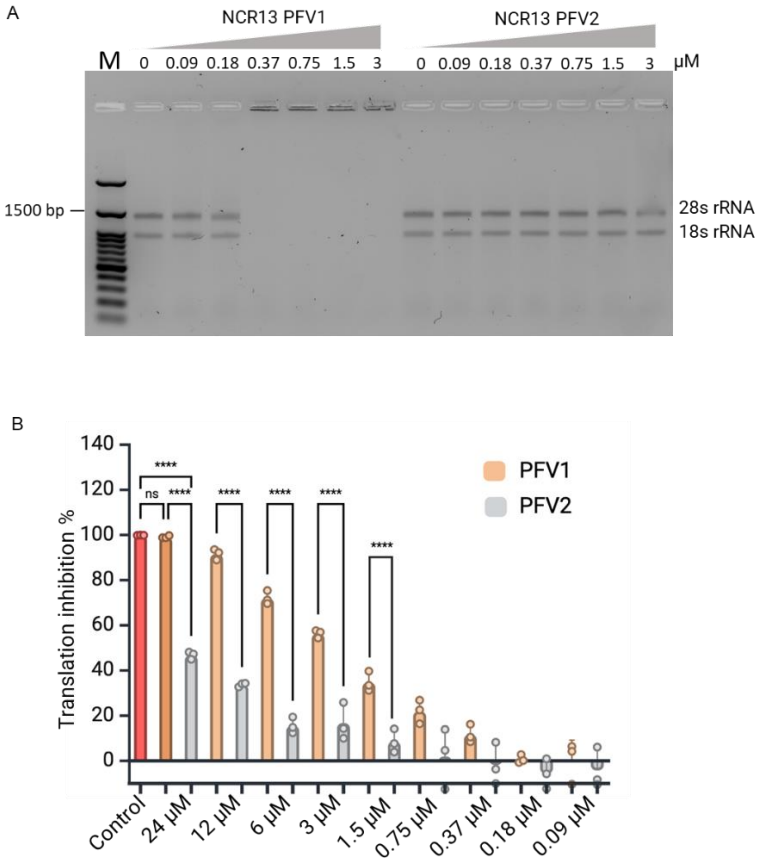

491

492 **Fig 9. NCR13_PFV1 exhibits rRNA binding and higher translation inhibition activity.** (A)
493 rRNA binding by NCR13_PFVs tested using electrophoretic mobility shift assay (EMSA). *Botrytis*
494 *cinerea* rRNA was used to assess the binding activity of the peptides NCR13_PFV1 and

495 NCR13_PFV2. The binding reactions were subjected to electrophoresis, and the mobility shifts
496 were visualized on an agarose gel (1%). The concentration gradient of peptides is indicated above
497 the lanes. The first lane on the left contains a molecular weight marker. (B) Relative *in vitro*
498 translational inhibition (%) in the presence of NCR13_PFVs at different concentrations. Sterile
499 water was used as negative control and cycloheximide (96 µM) was used as positive control. N=
500 3, 'N' indicates biological replicates. Statistical significance is determined using One-way ANOVA
501 with Tukey multiple comparisons test (**** indicates p value < 0.0001).
502

503 **NCR13_PFV1 is more potent than NCR13_PFV2 semi-*in planta***

504 Next, we compared the semi-*in planta* antifungal activity of NCR13_PFV1 and NCR13_PFV2
505 using detached leaves of pepper as previously described (31). To eliminate leaf-to-leaf variation,
506 both peptides were added instantaneously with freshly prepared *B. cinerea* spores to the same leaf,
507 along with a no-peptide control, at different concentrations (3, 1.5, and 0.09 µM) (S9A Fig). Leaves
508 were evaluated for reduction of gray mold lesions through measurement of photosynthetic
509 efficiency Fv/Fm (variable fluorescence over saturation level of fluorescence) using CropReporter
510 images. At 3 µM and 1.5 µM NCR13_PFVs, no disease symptoms were visualized (S9B Fig) and
511 no significant difference in photosynthetic efficiency (S9C Fig) was observed, whereas the no-
512 peptide control contained visible lesions and reduced photosynthetic efficiency. At 0.09 µM, only
513 NCR13_PFV1 effectively suppressed the formation of visible lesions, while NCR13_PFV2
514 resulted in lesion sizes similar to the no-peptide control (S9B Fig). Moreover, a decrease in
515 photosynthetic efficiency observed for NCR13_PFV1 was milder than observed for
516 NCR13_PFV2. Together, this data further illustrates that NCR13_PFV1 is a more potent antifungal
517 agent than NCR13_PFV2 in terms of preventing and reducing gray mold lesions on peppers (S9B
518 and C Fig). These observations correlate well with the *in vitro* antifungal activity of each peptide.
519 Based on this comparative study of their antifungal activity using a detached leaf assay,
520 NCR13_PFV1 was judged to be a more promising peptide-based fungicide *in planta* (see below).

521 **Spray-applied NCR13_PFV1 is more effective in reducing gray mold disease symptoms in**
522 **pepper and tomato plants**

523 To determine if the *in vitro* and semi-*in planta* antifungal activity of these peptides translated to
524 antifungal activity *in planta*, we tested the curative protection afforded by NCR13_PFV1 and
525 NCR13_PFV2 against *B. cinerea* by spray application on pepper plants. Four-week-old pepper
526 plants were pre-inoculated with freshly prepared *B. cinerea* spores. At 8 h post-inoculation, peptide
527 at 1.5 and 3 μM concentration was sprayed onto pepper leaves. At 72 h post-inoculation. disease
528 symptoms were evaluated by comparing photosynthetic efficiency (Fv/Fm) of the pathogen-
529 challenged peptide-sprayed plants with the no-peptide control. Green areas indicate a high
530 photosynthetic rate and healthy tissue, while yellow to red areas indicate reduced photosynthetic
531 rate and diseased tissue. As evidenced by their higher Fv/Fm values, leaves of pepper plants
532 sprayed with NCR13_PFV1 at 1.5 and 3 μM had greater reduction in gray mold lesions than the
533 leaves of pepper plants sprayed with NCR13_PFV2 at the same concentrations (Fig 10A and B).
534 Pepper plants sprayed with 1.5 μM NCR13_PFV2 showed no significant control ($p>0.05$) of gray
535 mold when compared to the no-peptide control plants suggesting NCR13_PFV2 is unable to
536 reduce gray mold disease symptoms at lower concentration (Fig 10A-C). Correspondingly, the
537 data aligns with the observation that NCR13_PFV1 markedly decreased the percentage of disease
538 severity relative to NCR13_PFV2 at both treatment concentrations (Fig 10C). However,
539 NCR13_PFV2 sprayed at 3 μM was able to provide significant curative protection compared to
540 control plants (Fig 10A-C), but it was not as effective as NCR13_PFV1. A similar observation was
541 made when four-week-old tomato plants were also pre-inoculated with *B. cinerea* spores followed
542 by spraying 3 μM of each peptide (S10A-C Fig). The NCR13_PFVs significantly decreased the
543 disease severity, with NCR13_PFV1 demonstrating the most pronounced effect (S10B Fig).

544 NCR13_PFV1 and NCR13_PFV2 inhibited gray mold disease 90% and 40%, respectively (S10C
545 Fig). In summary, these data indicate the higher curative antifungal potential of NCR13_PFV1 for
546 managing gray mold disease in pepper and tomato plants.

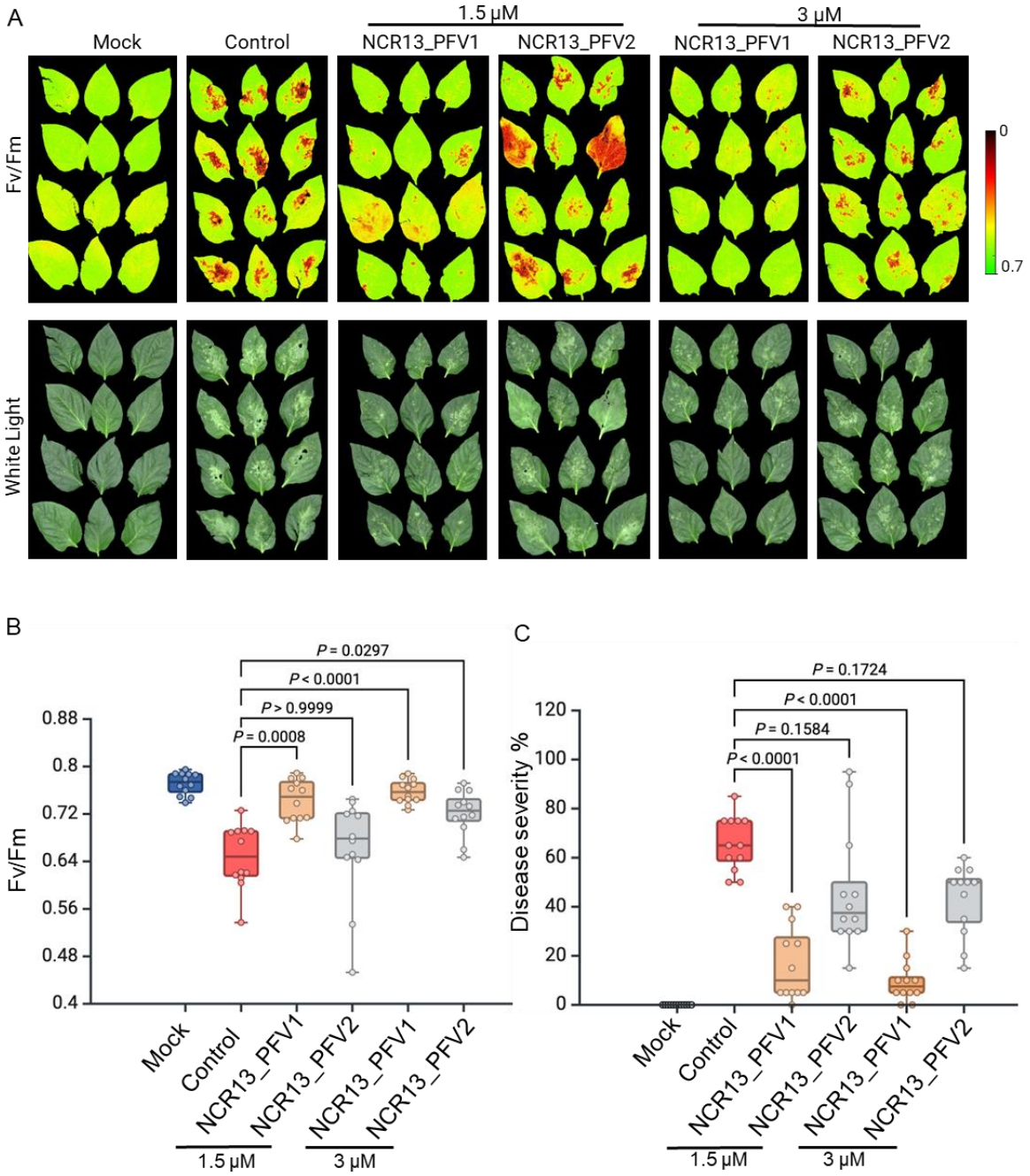

547

548 **Fig 10. NCR13 PFV1 exhibits enhanced curative antifungal activity against gray mold in**
549 **pepper (*Capsicum annuum*) plants.** (A) Curative antifungal activity of NCR13_PFV1 and PFV2.
550 Four-week-old pepper plants were first spray-inoculated using 1 mL of 5×10^4 *B. cinerea* spores.

551 At 8 hpi (hours post inoculation), the plants were sprayed with 2 mL of peptide (NCR13_PFV1 or
552 PFV2) at a concentration of 1.5 or 3 μM or control (*B. cinerea* alone). Mock-treated plants were
553 only sprayed with 1X SFM (no fungal spore suspension). (B) Calculated photosynthetic quantum
554 yield (Fv/Fm) for individual pepper plants. (C) Disease severity (%) was calculated as described
555 in materials and methods. (B-C) Each data point represents the average of 4 leaves per plant for 4
556 plants for each treatment. Horizontal lines represent the median and boxes indicate the 25th and
557 75th percentiles. The Kruskal-Wallis test with Dunn's multiple comparisons test is used to
558 determine statistically significant differences between control and peptide-treated inoculated
559 plants. Two independent experiments were performed with similar results.
560

561 **Discussion**

562 NCR13 is one of the highly cationic NCR peptides among the 63 found in chickpea nodules (10).
563 In this study, we discovered that NCR13 expressed in *P. pastoris* forms two isomers,
564 NCR13_PFV1 and NCR13_PFV2, which have identical amino acid sequence and molecular mass
565 but differ in their disulfide pairing patterns. We report a comparative analysis of the structure, *in*
566 *vitro* and semi-*in planta* antifungal activity and MoA of NCR13_PFVs. Our results support the
567 proposal that disulfide cross-linking provides an additional source of structural and functional
568 diversity in NCR peptides (21).

569 Four- or six-cysteine NCRs are highly diverse in their primary sequences and are predicted to
570 be structurally different. Previously, two solution NMR structures of NCR044 and NCR169, each
571 containing two disulfide bonds, were solved (19, 23). The NCR044 structure was largely
572 disordered, dynamic and contained a single α-helix and a β-sheet (19). Structural analysis revealed
573 that the two NCR169 isomers contained only one short, two-stranded β-sheet, with one isomer
574 being more extended and flexible while the other was more compact and constrained (23). To date,
575 a three-dimensional structure for a six-cysteine NCR peptide has not been reported. Here, we report
576 the first solution structures of two NCR13 disulfide isomers each containing an α-helix and β-
577 sheet. Nevertheless, unique pairing of two out of the three disulfide bonds significantly alters how

578 these secondary structure elements fold upon each other rendering NCR13_PFV1 more compact
579 and resistant to digestion by trypsin or reduction by dithiothreitol. It is striking that *P. pastoris*
580 generates two disulfide variants that are structurally different and raises the question of whether
581 these variants are also expressed in the differentiating nodules of chickpea to perform different
582 biological activities. In an earlier study, three disulfide variants of NCR247 containing four
583 cysteines were generated using chemical synthesis and *in vitro* folding. NCR247 variants were
584 found to have distinct patterns of biological activities such as bacterial gene expression, inhibition
585 of bacterial cell division, protein translation and antibacterial activity (21, 22). These observations
586 suggest that NCR peptides can form disulfide variants *in vitro* or in an appropriate expression host,
587 leading to diverse biological activity. Whether disulfide variants of NCR13, NCR247, or NCR169
588 are formed *in vivo* in nodules to control symbiosis in IRLC legumes remains an open question. In
589 contrast to NCR peptides, plant defensins with eight cysteines expressed in *P. pastoris* are only
590 observed as one species with an invariant disulfide pairing pattern (32).

591 To our knowledge, this study is the first detailed investigation of a chickpea NCR peptide and
592 its antifungal action. Our data demonstrates that disulfide folding variants of NCR13 produced in
593 *P. pastoris* exhibit profound differences in antifungal activity against multiple fungal pathogens of
594 economic importance. NCR13_PFV1 possesses highly potent antifungal activity against *B. cinerea*
595 and other pathogens, showing a four- to sixteen-fold greater activity compared to NCR13_PFV2.
596 Remarkably, we found that the antifungal activity of NCR13_PFV1 is greater than other NCR
597 peptides reported to date in literature (33). It is noteworthy that enhanced antifungal activity of
598 both NCR13_PFVs produced in *P. pastoris* compared to chemically synthesized NCR13 without
599 disulfide bond, underscores the critical role of disulfide bonds for antifungal activity. Furthermore,
600 the formation of all three disulfide bonds is essential for highly potent antifungal activity of

601 NCR13_PFV1 as removal of each disulfide bond resulted in a significant loss of its antifungal
602 activity against *B. cinerea*. In addition, Cys residues are essential for the antifungal activity of
603 NCR13 as their replacement with Ser leads to complete loss of antifungal activity. Acting as
604 molecular anchors, disulfide bonds provide stability to the three-dimensional structure of proteins
605 and peptides. They set the constraints for distance and angles between connected cysteine residues,
606 thus favoring the stability of the protein's folded state over its unfolded form (34). Furthermore,
607 the insertion of cysteine residues into *de novo* designed peptides has produced hyperstable peptides
608 with unique tertiary structures that form the basis for new peptide-based drugs (35, 36). The impact
609 on antifungal activity of knocking out two instead of just one disulfide bond is yet to be
610 investigated. Further, evaluating the three-dimensional structures of these double disulfide bond
611 knockout variants will provide deeper insight into structure-activity relationships of this unique
612 NCR peptide. *P. pastoris* has been the eukaryotic organism of choice for producing cysteine-rich
613 peptides to ensure formation of the correct disulfide bond patterns (37). It is intriguing that NCR13
614 expression results in the formation of two disulfide folding variants in *P. pastoris.* In this context,
615 it is critical to observe that knocking out either the C4-C23 or C15-C30 disulfide bond in
616 NCR13_PFV1 results in the formation of one peak on HPLC, whereas knocking out the C10-C28
617 bond still results in the formation of two distinct peaks. Mass spectrometry analysis shows that
618 peptides from two HPLC peaks of the C10-C28 knockout and one HPLC peak in the C4-C23 and
619 C15-C30 knockouts are in the oxidized state. Therefore, it is likely they are in a folded/oxidized
620 form. Finally, understanding the molecular mechanisms governing the generation of disulfide
621 variants of specific antifungal NCR peptides could pave the way for production of targeted
622 disulfide structural variants in *P. pastoris* with enhanced antifungal activity.

623 Antifungal peptides with potent fungicidal activity and multiple MoA are attractive candidates
624 for development as spray-on fungicides. NCR13 has a promise as one such candidate. For instance,
625 ability to permeabilize the plasma membrane of fungal pathogens is a common MoA of plant
626 cysteine-rich antifungal peptides including NCRs (14). NCR13_PFV1 can permeabilize the
627 plasma membrane of *B. cinerea* rapidly at very low concentrations. The membrane disrupting
628 ability of NCR13_PFV1 is far greater than that of NCR13_PFV2 and NCR044 (19). Both
629 NCR_PFVs bind to the same phospholipids on lipid strips with different binding intensity.
630 However, it is not clear what role, if any, phospholipid binding plays in conferring increased
631 membrane disrupting ability of NCR13_PFV1 and this aspect remains to be elucidated. In
632 addition, NCR13_PFV1 gains rapid entry into the interior of fungal cells compared to
633 NCR13_PFV2. It is plausible that more compact folding of NCR13_PFV1 allows it to more
634 quickly penetrate the cell wall and pass through the outer and inner leaflets of the plasma
635 membrane. This is supported by the fact that *B. cinerea* germlings challenged with 1.5 µM of each
636 peptide showed NCR13_PFV1 enters fungal cells in much greater levels after 2 h than
637 NCR13_PFV2. Moreover, once inside the cells, NCR13_PFV1 accumulates stably for at least 4 h
638 whereas NCR13_PFV2 tends to degrade in this time. Greater stability of NCR13_PFV1 to
639 proteolysis might be a major contributing factor to its much greater antifungal activity against this
640 pathogen, an observation that warrants further investigation.

641 Subcellular localization studies showed that NCR_PFVs are targeted to nucleoli in the
642 germlings of *B. cinerea* suggesting that these peptides are targeting ribosomal biogenesis or protein
643 translation machinery as part of their MoA as proposed earlier for the MoA of NCR044 (19). In
644 support of this hypothesis, we found that addition of each NCR13_PFVs to the *in vitro* translation
645 system inhibited protein synthesis in a concentration dependent manner. NCR13_PFV1 proved to

646 be more effective in inhibiting protein translation *in vitro*. NCR13_PFV1 also binds to *B. cinerea*
647 rRNA at a lower concentration (0.37 μM) than NCR13_PFV2 (6 μM). Further research is needed
648 to determine if differences in rRNA binding affinity and protein translation inhibition *in vitro*
649 directly translate to profound differences in their antifungal activity *in vivo*. NCR peptides appear
650 to target protein translation as part of their antimicrobial mechanism as evidenced by *M. truncatula*
651 NCR247 inhibiting protein translation *in vitro* by binding to ribosomal proteins (21, 38). Plant
652 defensin MtDef4 also inhibits protein translation *in vitro* by binding to ribosomal proteins, but not
653 to ribosomal RNA (39). Besides that, it is likely that NCR13_PFV1 and NCR13_PFV2 have
654 different, yet unidentified, intracellular targets which will be the subject of future investigation.

655 Fungicides currently used commercially for management of fungal diseases target ergosterol
656 biosynthesis, succinate dehydrogenase and cytochrome bc_1 complex. These targets are prone to
657 rapid development of fungal resistance (40). Small NCR peptides with multi-faceted MoA have
658 emerged as potential candidates for development as bioinspired fungicides. We have previously
659 demonstrated efficacy of NCR044 as a spray-on fungicide for management of gray mold in tomato
660 (19). Here, we report NCR13 is also a multi-target antifungal peptide that reduces gray mold
661 disease symptoms curatively when sprayed on pepper and tomato plants. Consistent with its *in*
662 *vitro* and semi-in planta antifungal activity, NCR13_PFV1 affords greater protection against gray
663 mold disease than NCR13_PFV2 in both pepper and tomato plants. NCR13 is amenable to large
664 scale recombinant production in a bio-fermenter using *P. pastoris* expression system. However,
665 further characterization of NCR13 is needed, including demonstrating its efficacy for control of
666 gray mold and other diseases in large-scale greenhouse and field tests, assessment of off-target
667 activity against mammalian cells and phytotoxicity. In summary, this study demonstrated that
668 disulfide bond pairing pattern has a profound impact on the *in vitro* antifungal activity, MoA, and

in planta antifungal activity of chickpea NCR13. As illustrated in Fig 11, the graphical abstract illustrates the key findings of our study. Overall, our work underscores the significance of disulfide cross-linking in enhancing the efficacy of antifungal peptides for agricultural use.

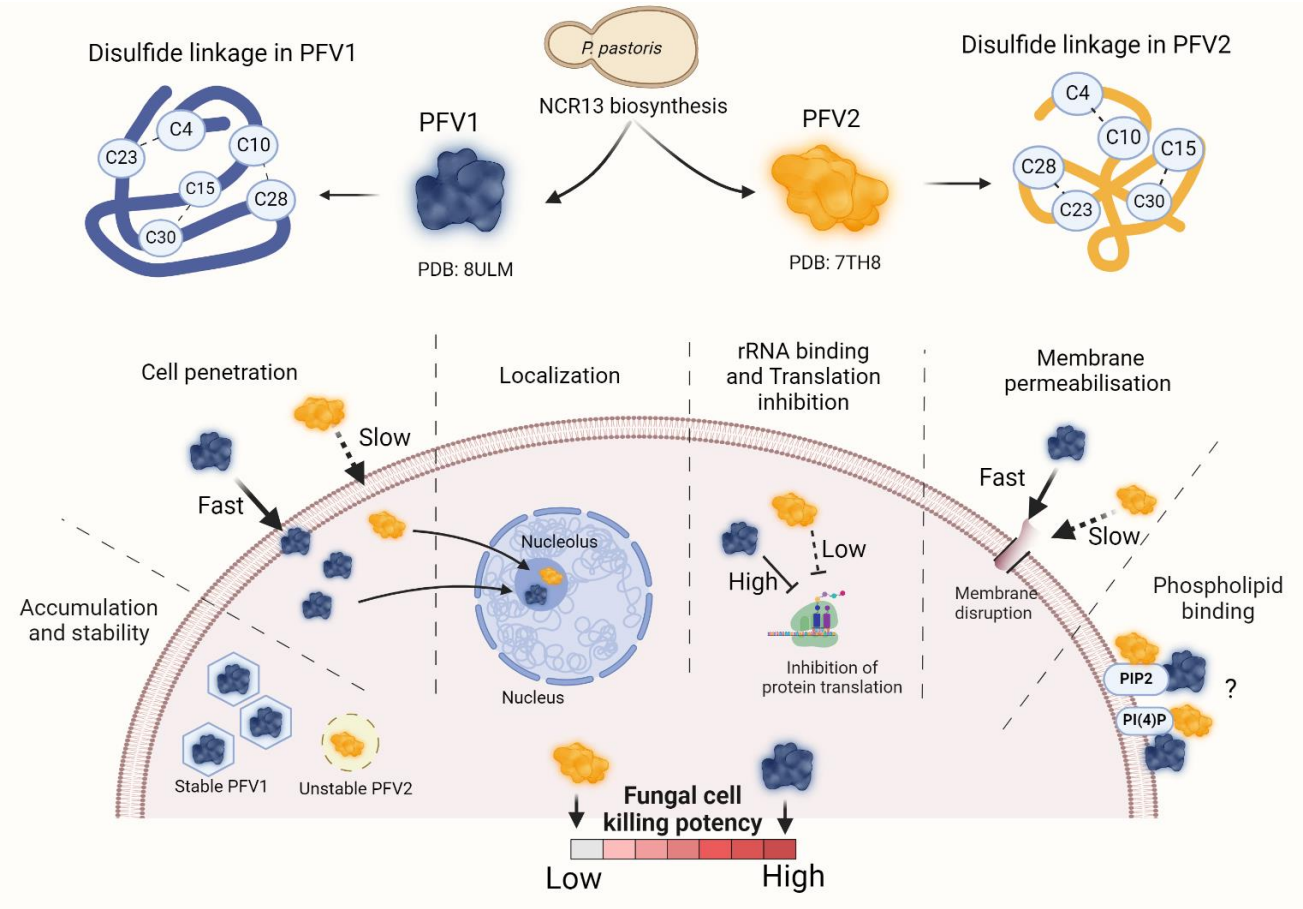

Fig 11. Graphical abstract illustrating the biosynthesis of disulfide linkage variants of NCR13 (PFV1 and PFV2) in *P. pastoris*, their structures, antifungal activity and modes of action in *B. cinerea* germlings. The figure depicts the differences in cell penetration, localization, rRNA binding and translation inhibition, membrane permeabilization, phospholipid binding, and overall fungal cell killing potency. Created using BioRender.com.

681 **Materials and Methods**

682 **Fungal Cultures and Spore Suspension**

683 *B. cinerea* strain T4 was cultured in V8 medium for 3 weeks at 25°C. Fungal spores were collected
684 by flooding the fungal growth plates with water and scraped using sterile spreader. The spore
685 suspension was filtered through two layers of Miracloth, followed by centrifugation at 12,000 g
686 for 2 minutes (min) and subsequently washed twice with sterile water. Lastly, fungal spores were
687 resuspended in Synthetic Fungal Media (SFM) (41). The spore suspension was adjusted to the
688 desired spore density of about 10^5 spores/mL using a hemocytometer. *Fusarium virguliforme (F.*
689 *virguliforme*) was grown and maintained regularly in potato dextrose agar (PDA) (Difco
690 Laboratories) medium. Two weeks old *F. virguliforme* plates were used to collect spores as
691 described above for *B. cinerea* followed by centrifugation and washing step. Spores were counted
692 using a hemocytometer and adjusted to the final concentration of 10^5 spores/mL in 2X SFM media.
693 *Sclerotinia sclerotiorum* obtained from the field of pennycress in Illinois was grown on PDA
694 medium at room temperature.

695 **Expression and purification of NCR13**

696 For expression in *P. pastoris*, the published amino acid sequence of the mature NCR13 peptide
697 (24) was used for synthesis of the codon-optimized gene (GenScript). The NCR13 gene was
698 expressed in *P. pastoris* X33 using either a SacI linearized pPICZα-A integration vector
699 (Invitrogen) or at XhoI and XbaI restriction sites. NCR13 was purified using a CM Sephadex C-
700 25 cation-exchange chromatography as described (19). After induction, cell-free supernatant was
701 collected after centrifugation (10,000×g) at 4 °C for 20 min, and the pH was adjusted to 6.0. The
702 supernatant was passed through cation-exchange resin, CM Sephadex C-25 (Sigma-Aldrich, Cat
703 No: C25120) previously equilibrated with binding buffer (25 mM Sodium Acetate Anhydrous, pH

704 6.0) using an AKTA FPLC. Peptides bound to the resin were eluted using the elution buffer (1M
705 NaCl, 50 mM Tris, pH 7.6). The FPLC fraction containing NCR13 was concentrated and desalted
706 using an Amicon Stirred Cell with a 3-kD cutoff membrane (Millipore, Cat No: PLBC04310) and
707 further purified by reverse phase C18-HPLC. HPLC fractions collected separately for
708 NCR13_PFV1 and NCR13_PFV2 were lyophilized and re-suspended in nuclease-free water.
709 Peptide concentrations were determined using the Pierce™ BCA Protein Assay Kit (Thermo
710 Scientific). NCR13 and alanine variants of NCR13 were chemically synthesized (Biomatik) and
711 further purified by in-house HPLC.

712 **Molecular weight determination**

713 Purified peptides were analyzed by LC-MS for accurate mass determination. Firstly, peptide
714 samples were cleaned using Thermo Scientific HyperSep C18 microscale SPE extraction tips and,
715 after dry-down, resuspended in 0.1% formic acid for LC-MS analysis. LC-MS was performed with
716 a Dionex RSLCnano HPLC coupled to an OrbiTrap Fusion Lumos (Thermo Scientific) mass
717 spectrometer using 80 min gradient (1-90% acetonitrile). Sample was resolved using a 75 µm x 15
718 cm PepMap C18 column (Thermo Scientific). MS spectra of protein ions of different charge-states
719 were acquired in positive ion mode with a resolution setting of 120,000 (at m/z 200). Mass
720 deconvolution was performed using ProteinProspector, Xcalibur (Thermo Scientific), and ESIprot
721 Online.

722 **Disulfide bond pattern identification for NCR13_PFV2 using mass spectrometry**

723 An aliquot of unlabeled, oxidzed NCR13_PFV2 was mixed with 20-fold less (in mass) trypsin,
724 incubated at room temperature for 1 h, and diluted in 50% acetonitrile, 0.1% formic acid to ~0.1
725 µM. The diluted samples were infused at 2 µL/min into a Thermo Q-Exactive Exploris 480
726 Orbitrap mass spectrometer with positive mode electrospray at 3.4 kV. The ion transfer tube was

727 at 320 °C, sheath gas at 2 psi, and auxiliary gas at 5 psi. Data-dependent acquisition was used
728 (MS1 resolution 60k, MS2 resolution 30k) over 8 min. Fragmentation spectra were collected with
729 higher-energy collisional dissociation (HCD) at 30% collision energy. Data were analyzed and
730 deconvoluted in FreeStyle (Thermo Scientific). Crosslinked peptides were identified using Byonic
731 (ProteinMetrics). Under the same conditions, NCR13_PFV1 could not be digested by trypsin.

732 **^{15}N isotopic labeling of NCR13 for NMR structural analysis**

733 The ^{15}N-labeled NCR13_PFVs were prepared according to the protocol as described previously
734 (32) with minor modifications. NCR13-expressing *P. pastoris* X33 was grown at 28 ± 2˚C for two
735 days on a YPD plate containing 150 µg/mL Zeocin. A single colony was then inoculated into 5 mL
736 of YPD broth and grown overnight at 28 ± 2 ˚C on a rotary shaker at 225 ± 25 rpm. After overnight
737 growth, a 5 mL culture was transferred aseptically to 100 mL of FM23 medium (0.8% YNB
738 without amino acids and ammonium sulfate, 2 mg/L biotin, 1.2% $(NH_4)_2SO_4$, 0.3% K_2HPO_4,
739 0.28% KH_2PO_4, 2 ml/L PTM1 salts) containing 3% glucose. After 24 h, an additional 2% glucose
740 was added to the culture medium. After a growth phase of ~30 h and just prior to methanol
741 induction, the culture medium was adjusted to 0.02% ^{15}N-ammonium chloride ($^{15}NH_4Cl$) and 0.1%
742 glucose. After 40 h, cells were harvested by centrifugation at 5,000 rpm at room temperature for
743 10 min, briefly washed with 0.2% glycerol, pelleted, and re-suspended in 100 mL FM23 medium
744 containing 1.2% $^{15}NH_4Cl$ and grown for 4-5 days at 25 ˚C at 225 ± 25 rpm. In the induction phase,
745 a low concentration of 0.2% methanol was initially added to the culture medium to induce protein
746 expression and gradually increased by 0.4% from 72 to 120 h (1.4% final). The labeled NCR13
747 peaks were purified from the *P. pastoris* growth medium following the same protocol used for the
748 unlabeled peptide.

749

750 **NMR spectroscopy of NCR13**

751 All NMR data were collected at 20˚C on ^{15}N-labeled samples of oxidized NCR13_PFV1 and
752 NCR13_PFV2 (~ 1 mM, 20 mM sodium acetate, 50 mM NaCl, pH 5.3) using Varian (Inova-600)
753 or Bruker (Advent-750) spectrometers equipped with an HCN-probe and pulse field gradients.
754 Except for the carbonyl resonances (which could not be assigned because making ^{13}C-labeled
755 samples in *P. pastoris* was too expensive), the ^{1}H, ^{13}C, and ^{15}N chemical shifts of the backbone
756 and side chain resonances were assigned from the analysis of two-dimensional ^{1}H-^{15}N HSQC, ^{1}H-
757 ^{13}C HSQC, ^{1}H-^{1}H TOCSY, ^{1}H-^{1}H NOESY, and ^{1}H-^{1}H COSY spectra and three-dimensional ^{15}N-
758 edited NOESY-HSQC (mixing time = 90 ms) and ^{15}N-edited TOCSY spectra. To obtain additional
759 chemical shift assignments, inter- and intra-residue proton side chain restraints for proton near the
760 residual water resonance, most of the two-dimensional data sets were also collected by lyophilizing
761 and resuspending the sample in 99.8% D_2O. In preparing the latter sample, a ^{1}H-^{15}N HSQC
762 spectrum was collected ~10 min after the addition of D_2O to identify slowly exchanging amides
763 that could be used as hydrogen bond restraints in the structure calculations. To confirm oxidized
764 NCR13_PFV1 and NCR13_PFV2 arose from different disulfide bond patterns of a common
765 precursor primary amino acid sequence, both oxidized samples were reduced by making the NMR
766 samples 5 mM in Dithiothreitol (DTT). While NCR13_PFV2 was reduced rapidly, it took more
767 than 5 – 7 days to fully reduce NCR13_PFV1. All NMR data were processed using Felix 2007
768 (MSI, Molecular Simulations) software and analyzed with the program Poky (v3.115) (42). The
769 assigned ^{1}H, ^{13}C, and ^{15}N chemical shifts were referenced using indirect methods (DSS = 0 ppm)
770 and deposited into the BioMagResBank database (www.bmrb.wisc.edu) under the accession
771 numbers BMRB-31111 (oxidized NCR13_PFV1 8ULM) and BMRB-30979 (oxidized
772 NCR13_PFV2 7TH8).

773 **NMR solution structure calculations for oxidized NCR13_PFV1 and NCR13_PFV2**

774 The protocols used to obtain solution structures for both peptides followed a similar approach
775 starting with the ^{1}H, and ^{15}N chemical shift assignments and peak-picked NOESY data serving as
776 initial experimental inputs in iterative structure calculations with the program CYANA (v 2.1) (43).
777 The ^{1}H, ^{13}C, and ^{15}N chemical shift assignments were also the primary basis for the introduction
778 of 24 (NCR13_PFV1) and 25 (NCR13_PFV2) dihedral Psi (ψ) and Phi (φ) angle restraints
779 identified with the program TALOS+ using the online webserver
780 (https://spin.niddk.nih.gov/bax/nmrserver/talos/) (44). Nine restraints between the side chain
781 sulfur atoms of C4-C23, C15-C30, and C10-C28 (NCR13_PFV1) and C4-C10, C15-C30, and
782 C23-C28 (NCR13_PFV1) (2.0-2.1 Å, 3.0-3.1 Å, and 3.0-3.1 Å for the Sγ-Sγ, Sγ-Cβ, and Cβ-Sγ
783 distances, respectively) (19, 45) were introduced on the basis of AlphaFold predictions for
784 NCR13_PFV1 and high resolution mass spectrometry analysis for NCR13_PFV2. Exhaustive
785 attempts to identify the disulfide bond pattern for NCR13_PFV1 using various mass spectrometric
786 methods failed likely due to its hyperstability to reduction by DTT or tris(2-carboxyethyl)
787 phosphine. Backbone hydrogen bond restraints (1.8 – 2.0 Å and 2.7 – 3.0 Å for the NH–O and N-
788 O distances, respectively) were added to the calculations for proximate backbone amide-carbonyl
789 groups present in early structure calculations that were accompanied with slowly exchanging
790 amides in the deuterium exchange experiment. The final ensemble of 20 CYANA derived
791 structures was then refined in explicit water with CNS (version 1.1) using the PARAM19 force
792 field and force constants of 500, 500, and 1000 kcal for the NOE, hydrogen bond, and dihedral
793 restraints, respectively. For these water refinement calculations, 10 and 0 % were added to the
794 upper boundary of the CYANA distance restraints for NCR13_PFV1 and NCR13_PFV2,
795 respectively, and the lower boundary set to the van der Waals limit for both. Structural quality was

796 assessed using the online Protein Structure Validation Suite (PSVS, v1.5) (46). Complete structural
797 statistics are summarized in S3 Table. The atomic coordinates for the final ensemble of 20
798 structures have been deposited in the Research Collaboratory for Structural Bioinformatics
799 (RSCB) under PDB codes 8ULM (NCR13_ PFV1) and 7TH8 (NCR13_ PFV2).

800 **Peptide uptake and stability assessment within *B. cinerea***

801 *B. cinerea* (~10^5 spores/mL) was inoculated in 10 mL of Potato Dextrose Broth (PDB) and
802 incubated in a shaker at 28ºC for 18 h. *B. cinerea* germlings were treated with 1.5 µM
803 NCR13_PFV1 and NCR13_PFV2 for 0, 2 and 4 h. Total proteins were extracted from the fungal
804 cells using 300 µL of HEPES buffer (100 mM HEPES, 5mM EDTA, 0.1% Triton-100, ProBlock™
805 Gold Yeast/Fungi Protease Inhibitor, pH 7.5) and centrifuged at 14000 rpm to remove cell debris.
806 The concentration of protein present in the supernatant was measured using Pierce™ BCA Protein
807 Assay Kit (Thermo Scientific). Total proteins (10 µg) were separated on a 4–20% SDS-PAGE gel
808 (Bio-Rad, TGX Stain-Free™ precast gels) and transferred to a nitrocellulose membrane. Equal
809 loading of proteins was checked using Ponceau S staining (Thermo Scientific). Immunoblotting
810 was performed using the custom synthesized anti-NCR13 polyclonal antibody (Biomatik) at a
811 concentration of 0.1 µg/mL followed by an incubation in the secondary anti-rabbit antibody
812 (Cytiva, Cat No: RPN4301) with a dilution of 1:20,000.

813 ***In vitro* antifungal assay**

814 The antifungal activity of NCR13 against fungal pathogens was determined using the resazurin
815 cell viability assay as described previously (47). Briefly, 45 µL of each peptide dilution (0, 0.09,
816 0.1875, 0.375, 0.75, 1.5, 3 and 6 µM) was added to each well of the microtiter plate containing 45
817 µL (~10^5 spores/mL) of spore suspension. Three biological replicates were used for each treatment
818 and the experiments were repeated three times. Resazurin at 0.1% (w/v) was added to each well

819 after incubation for 48 h. Images were taken at ~24 h. The Minimum Inhibitory Concentration
820 (MIC) for each peptide denotes the lowest concentration at which the peptide halts the growth of
821 fungus evident through a lack of color change from blue to colorless. The *in vitro* antifungal
822 activity of NCR13_PFVs against *S. sclerotiorum* was determined using a 24-well plate assay as
823 described (48). Mycelial plugs (1 mm in diameter) cut from the growing edge of the two-day-old
824 actively growing colony were transferred from PDA media to a series of wells containing 250 µL
825 of SFM.

826 **Internalization and permeabilization assays using confocal microscopy**

827 NCR13_PFV1 and PFV2 were labeled with DyLight550 amine reactive fluorescent dye following
828 the manufacturer's instructions (Thermo Scientific). *B. cinerea* germlings (50 µL, ~$5x10^4$
829 spores/mL) were treated with DyLight 550 labeled NCR13_PFV1 and NCR13_PFV2 (50 µL, 0.09
830 µM and 1.5 µM), and the fluorescence measured with excitation and emission wavelengths of 550
831 and 560-600 nm, respectively. Time-lapse confocal microscopy data with a z-stack at each time
832 point were acquired using a 63X water immersion objective lens (HC PL Apochromat CS2) at 30-
833 second intervals. For the membrane permeabilization assay, fluorescent dye SYTOX™ Green
834 (Thermo Scientific) at a concentration of 0.25 µM was used to determine the membrane
835 permeabilization of *B. cinerea* germlings as described previously (31). Time lapse imaging was
836 performed to visualize the SYTOX™ Green entry upon treatment with 50 µL of 0.09 and 1.5 µM
837 NCR13_PFVs. Imaging was performed on a Leica SP8 confocal microscope with excitation at 488
838 nm and emission at 508–544 nm. Average fluorescence intensity measurements were obtained
839 using Fiji (49).

840

841

Phospholipid binding assays

Phospholipid binding of NCR13_PFVs were performed with PIP Strips (Echelon Biosciences, Cat No: P-6001) that are spotted with 100 pmol of various biologically active phospholipids. Peptide binding to the membrane strips was detected using monoclonal NCR13 antibody (0.1 µg/mL) followed by goat anti-rabbit IgG HRP (Cytiva RPN4301) at 1:20,000 dilution. The binding signals were detected using the SuperSignal West Pico Chemiluminescent Substrate Kit (Thermo Scientific) following the manufacturer's protocol. Quantitative analysis of the blot intensity was performed using Fiji (49).

Oligomerization assay

To determine the oligomerization status of the NCR13_PFVs, the peptides were prepared in PBS buffer at 1.5 mg/mL (5 µL/reaction) and incubated with specified concentrations of PI(4,5)P2. The cross-linking reaction was initiated by addition of 12.5 mM bis(sulfosuccinimidyl)suberate BS3 (Thermo Scientific) and then incubated for 30 min at room temperature. After incubation, tricine sample buffer was added to each sample and heat denatured at 95 ºC for 5 min. Samples were loaded on a 16.5% Tris-Tricine precast gel (Bio-Rad Laboratories). For SDS-PAGE, 5 µL of Precision Plus Dual Xtra Protein Standards (2–250 kDa) were used (Bio-Rad Laboratories). Oligomerization patterns were visualized using silver staining.

PolyPIPosome binding assay

The validation of the binding of NCR13_PFV1 and NCR13_PFV2 to phospholipids was further performed using a liposome binding assay. In this assay, polyPIPosome binding was conducted in 200 µL of binding buffer (20 mM HEPES pH 7.4, 120 mM NaCl, 1 mM EGTA, 1 mM $MgCl_2$, 1 mg/mL BSA, 0.2 mM $CaCl_2$, 5 mM KCl) plus 10 µL each of control PolyPIPosome, PI4P PolyPIPosomes, and PIP_2 PolyPIPosome (Echelon Biosciences). Subsequently, 2 µg of each

peptide was added, and the mixture incubated for 1 h at room temperature. Following incubation, liposomes were collected by centrifugation at 16,000 × g for 20 min, and the supernatant was collected. The pellet was subjected to three washes in 1 mL of binding buffer. After the washes, the pellet was resuspended in 40 µL of 2X Laemmli sample buffer. Both samples were reduced with 100 mM DTT and separated on a 4–20% TGX Stain-Free™ precast gels (Bio-Rad Laboratories). Proteins were then transferred to a nitrocellulose membrane and subjected to blotting using the NCR13 antibody.

Electrophoretic mobility shift assay

Total RNA was extracted and purified from *B. cinerea* grown in Potato Dextrose Broth (Fisher Scientific) using the NucleoSpin RNA Plus Mini kit (Takara Bio) according to manufacturer instructions. The gel shift experiments were performed by mixing 200 ng of the total RNA with different concentrations of NCR13 PFV1 and PFV2 (0-3 µM) in 20 µL of binding buffer (10 mM Tris-HCl, pH 8.0, 1 mM EDTA). The reaction mixtures were incubated for 1 h at room temperature and mixed with 4 µL of 6X gel loading dye (New England Biolabs). Following electrophoresis in 1.2% agarose gel containing SYBR safe DNA gel stain (Thermo Scientific) with TAE buffer at 120 V for 45 min, the gels were visualized using a Bio-Rad ChemiDoc XRS+ system.

***In vitro* translation assay**

In vitro translation was performed using the RiboMAX™ Large Scale RNA Production system and Wheat Germ Extract *in vitro* translation system (Promega). First, the luciferase DNA template (Promega) was transcribed to mRNA and translated to luciferase following the manufacturer's protocol. The luciferase enzyme activity was detected by the luciferase kit (Promega) using a luminometer (Tecan). Different concentrations of NCR13_PFV1 and NCR13_PFV2 were used to determine their translation inhibition ability. Sterile water was added to the *in vitro* translation

888 system as a negative control and a fungal translation inhibitor cycloheximide (48 μM) was used as
889 a positive control. Translation inhibition (TI) percentage is calculated using this formula TI % =
890 (1− a/b) x 100, where 'a' equals the translation level with peptide and 'b' equals the translation
891 level without peptide.

892 ***In planta* and Semi-*In planta* antifungal assays**

893 Pepper (*Capsicum annuum*, California Wonder 300 TMR) plants used in this study were grown in
894 a greenhouse for 4 weeks under 14 h light/10 h dark cycle. Tomato (*Solanum lycopersicum* cv.
895 Mountain Spring) plants were grown in a controlled environment growth chamber for 4 weeks,
896 under a 16 h light/ 8 h dark cycle. Semi-*in planta* antifungal activity of each peptide against *B.*
897 *cinerea* was determined using detached leaves of pepper. NCR13_PFV1 and NCR13_PFV2 were
898 tested at 6, 1.5, and 0.09 μM. Following incubation of 10 μL peptide with 10 μL of *B. cinerea*
899 spores (~10^5 spores/mL) under a humid environment for 48 h, the leaves were photographed in
900 white light. High-resolution fluorescence images were also taken using CropReporter
901 (PhenoVation). These images depicted the calculated Fv/Fm (maximum quantum yield of
902 photosystem II) values of the diseased area affected by *B. cinerea* infection. Colors in the images
903 show five different classes ranging from class I to class V (0.000 to 0.700) depicting varying
904 degrees of tissue damage.

905 To test the curative antifungal activity of peptides against *B. cinerea*, 4-week-old pepper and
906 tomato plants were used. Plants were first sprayed with 1 mL of *B. cinerea* spores (about 5×10^4)
907 suspended in 1× SFM. After 8 h of *B. cinerea* challenge, 2 mL of NCR13_PFV1 or NCR13_PFV2
908 (3.0 and 1.5 μM) were sprayed per plant. Control plants were sprayed with 2 mL of water. All
909 plants were placed in a high humid environment for 72 h. Plants were imaged at 72 h after infection
910 in white light and high-resolution fluorescence images were taken using CropReporter

(PhenoVation). The quantification of plant health was carried out using the calculated Fv/Fm (maximum quantum yield of photosystem II) images of the CropReporter showing the efficiency of photosynthesis in false colors.

For the curative assay using pepper and tomato plants, the picture of the whole plants and detached leaves were taken as described above. The disease symptoms on individual leaves of each plant, were visually assessed in % of disease portion (disease severity) and on a rating scale of 0-5 where each rank would represent the following proportion of diseased tissue per leaf : Scale 0: No obvious signs/symptoms of disease, Scale 1: $0 > x \leq 20$ % diseased portion of leaf, Scale 2: $20 > x \leq 40$ % diseased portion of leaf, Scale 3: $40 > x \leq 60$ % diseased portion of leaf, Scale 4: $60 > x \leq 80$ % diseased portion of leaf, Scale 5: $80 > x \leq 100$ % diseased portion of leaf. Four plants were used per treatment and for each plant the disease was assessed per leaf. Besides disease severity (DS), the inhibition of disease by treatment was also evaluated. The following formula was used to assess the inhibition of disease severity by each treatment: % Disease Inhibition= (Average DS for Control -Treatment DS)/(Average DS for Control) x 100%. Where treatment DS is the disease severity for each leaf except those of the control. Plots were generated using the 'ggplot2' package in R version 4.3.2.

References

1. McLaughlin MS, Roy M, Abbasi PA, Carisse O, Yurgel SN, Ali S. Why Do We Need Alternative Methods for Fungal Disease Management in Plants? Plants (Basel). 2023;12(22).
2. Goyal RK, Mattoo AK. Multitasking antimicrobial peptides in plant development and host defense against biotic/abiotic stress. Plant Sci. 2014;228:135-49.
3. Dos Santos-Silva CA, Zupin L, Oliveira-Lima M, Vilela LMB, Bezerra-Neto JP, Ferreira-Neto JR, et al. Plant Antimicrobial Peptides: State of the Art, In Silico Prediction and Perspectives in the Omics Era. Bioinform Biol Insights. 2020;14:1177932220952739.
4. van der Weerden NL, Bleackley MR, Anderson MA. Properties and mechanisms of action of naturally occurring antifungal peptides. Cellular and molecular life sciences : CMLS. 2013;70(19):3545-70.
5. Lobo F, Boto A. Host-defense peptides as new generation phytosanitaries: Low toxicity and low induction of antimicrobial resistance. Agronomy. 2022;12:1614.
6. Tavormina P, De Coninck B, Nikonorova N, De Smet I, Cammue BP. The Plant Peptidome: An Expanding Repertoire of Structural Features and Biological Functions. Plant Cell. 2015;27(8):2095-118.
7. Cools TL, Struyfs C, Cammue BP, Thevissen K. Antifungal plant defensins: increased insight in their mode of action as a basis for their use to combat fungal infections. Future Microbiol. 2017;12:441-54.
8. Maroti G, Downie JA, Kondorosi E. Plant cysteine-rich peptides that inhibit pathogen growth and control rhizobial differentiation in legume nodules. Current opinion in plant biology. 2015;26:57-63.
9. Parisi K, Shafee TMA, Quimbar P, van der Weerden NL, Bleackley MR, Anderson MA. The evolution, function and mechanisms of action for plant defensins. Semin Cell Dev Biol. 2019;88:107-18.
10. Montiel J, Downie JA, Farkas A, Bihari P, Herczeg R, Balint B, et al. Morphotype of bacteroids in different legumes correlates with the number and type of symbiotic NCR peptides. Proc Natl Acad Sci U S A. 2017;114(19):5041-6.
11. Kondorosi E, Mergaert P, Kereszt A. A paradigm for endosymbiotic life: cell differentiation of Rhizobium bacteria provoked by host plant factors. Annu Rev Microbiol. 2013;67:611-28.
12. Kereszt A, Mergaert P, Montiel J, Endre G, Kondorosi E. Impact of Plant Peptides on Symbiotic Nodule Development and Functioning. Front Plant Sci. 2018;9:1026.
13. Mergaert P. Role of antimicrobial peptides in controlling symbiotic bacterial populations. Nat Prod Rep. 2018;35(4):336-56.
14. Ordogh L, Voros A, Nagy I, Kondorosi E, Kereszt A. Symbiotic plant peptides eliminate Candida albicans both in vitro and in an epithelial infection model and inhibit the proliferation of immortalized human cells. Biomed Res Int. 2014;2014:320796.
15. Farkas A, Maroti G, Kereszt A, Kondorosi E. Comparative Analysis of the Bacterial Membrane Disruption Effect of Two Natural Plant Antimicrobial Peptides. Frontiers in microbiology. 2017;8:51.
16. Tiricz H, Szűcs A, Farkas A, Pap B, Lima RM, Maróti G, et al. Antimicrobial Nodule-Specific Cysteine-Rich Peptides Induce Membrane Depolarization-Associated Changes in the Transcriptome. Applied and Environmental Microbiology. 2013;79(21):6737.
17. Balogh EP, Mosolygo T, Tiricz H, Szabo AM, Karai A, Kerekes F, et al. Anti-chlamydial effect of plant peptides. Acta Microbiol Immunol Hung. 2014;61(2):229-39.

18. Alhhazmi AA, Alluhibi SS, Alhujaily R, Alenazi ME, Aljohani TL, Al-Jazzar AA, et al. Novel antimicrobial peptides identified in legume plant, Medicago truncatula. Microbiol Spectr. 2024;12(2):e0182723.
19. Velivelli SLS, Czymmek KJ, Li H, Shaw JB, Buchko GW, Shah DM. Antifungal symbiotic peptide NCR044 exhibits unique structure and multifaceted mechanisms of action that confer plant protection. Proc Natl Acad Sci U S A. 2020;117(27):16043-54.
20. Bulleid NJ, Ellgaard L. Multiple ways to make disulfides. Trends Biochem Sci. 2011;36(9):485-92.
21. Shabab M, Arnold MF, Penterman J, Wommack AJ, Bocker HT, Price PA, et al. Disulfide cross-linking influences symbiotic activities of nodule peptide NCR247. Proc Natl Acad Sci U S A. 2016;113(36):10157-62.
22. Haag AF, Kerscher B, Dall'Angelo S, Sani M, Longhi R, Baloban M, et al. Role of cysteine residues and disulfide bonds in the activity of a legume root nodule-specific, cysteine-rich peptide. J Biol Chem. 2012;287(14):10791-8.
23. Isozumi N, Masubuchi Y, Imamura T, Mori M, Koga H, Ohki S. Structure and antimicrobial activity of NCR169, a nodule-specific cysteine-rich peptide of Medicago truncatula. Sci Rep. 2021;11(1):9923.
24. Montiel J, Szucs A, Boboescu IZ, Gherman VD, Kondorosi E, Kereszt A. Terminal Bacteroid Differentiation Is Associated With Variable Morphological Changes in Legume Species Belonging to the Inverted Repeat-Lacking Clade. Mol Plant Microbe Interact. 2016;29(3):210-9.
25. Yee A, Chang X, Pineda-Lucena A, Wu B, Semesi A, Le B, et al. An NMR approach to structural proteomics. Proc Natl Acad Sci U S A. 2002;99(4):1825-30.
26. Shaw WJ, Tarasevich BJ, Buchko GW, Arachchige RMJ, Burton SD. Controls of nature: Secondary, tertiary, and quaternary structure of the enamel protein amelogenin in solution and on hydroxyapatite. J Struct Biol. 2020;212(3):107630.
27. Jumper J, Evans R, Pritzel A, Green T, Figurnov M, Ronneberger O, et al. Highly accurate protein structure prediction with AlphaFold. Nature. 2021;596(7873):583-9.
28. Poon I, Baxter AA, Lay FT, Mills GD, Adda CG, Payne JA, et al. Phosphoinositide-mediated oligomerization of a defensin induces cell lysis. eLife. 2014;3:e01808.
29. Hellman LM, Fried MG. Electrophoretic mobility shift assay (EMSA) for detecting protein-nucleic acid interactions. Nature protocols. 2007;2(8):1849-61.
30. Olliver CL, Grobler-Rabie A, Boyd CD. In vitro translation of messenger RNA in a wheat germ extract cell-free system. Methods Mol Biol. 1985;2:137-44.
31. Li H, Velivelli SL, Shah DM. Antifungal potency and modes of action of a novel olive tree defensin against closely related ascomycete fungal pathogens. . Mol Plant Microbe Interact. 2019;32:164901664.
32. Kovaleva V, Bukhteeva I, Kit OY, Nesmelova IV. Plant Defensins from a Structural Perspective. Int J Mol Sci. 2020;21(15).
33. Lima RM, Kylarova S, Mergaert P, Kondorosi E. Unexplored Arsenals of Legume Peptides With Potential for Their Applications in Medicine and Agriculture. Front Microbiol. 2020;11:1307.
34. Wedemeyer WJ, Welker E, Narayan M, Scheraga HA. Disulfide bonds and protein folding. Biochemistry. 2000;39(23):7032.
35. Bhardwaj G, Mulligan VK, Bahl CD, Gilmore JM, Harvey PJ, Cheneval O, et al. Accurate de novo design of hyperstable constrained peptides. Nature. 2016;538(7625):329-35.
36. Buchko GW, Pulavarti S, Ovchinnikov V, Shaw EA, Rettie SA, Myler PJ, et al. Cytosolic expression, solution structures, and molecular dynamics simulation of genetically encodable disulfide-rich de novo designed peptides. Protein Sci. 2018;27(9):1611-23.

37. Karbalaei M, Rezaee SA, Farsiani H. Pichia pastoris: A highly successful expression system for optimal synthesis of heterologous proteins. J Cell Physiol. 2020;235(9):5867-81.
38. Farkas A, Maroti G, Durgo H, Gyorgypal Z, Lima RM, Medzihradszky KF, et al. Medicago truncatula symbiotic peptide NCR247 contributes to bacteroid differentiation through multiple mechanisms. Proc Natl Acad Sci U S A. 2014;111(14):5183-8.
39. Li H, Kalunke R, Tetorya M, Czymmek KJ, Shah DM. Modes of action and potential as a peptide-based biofungicide of a plant defensin MtDef4. Mol Plant Pathol. 2024;25, e134538. https://doi.org/10.1111/mpp.134538.
40. Hawkins NJ, Fraaije BA. Fitness Penalties in the Evolution of Fungicide Resistance. Annu Rev Phytopathol. 2018;56:339-60.
41. Liang J, Shah DM, Wu Y, Rosenberger CA, Hakimi SM, inventors; Monsanto Company, assignee. Antifungal polypeptide from alfalfa and methods for controlling plant pathogenic fungi. USA patent US 6316407. 2001 November 13, 2001.
42. Lee W, Rahimi M, Lee Y, Chiu A. POKY: a software suite for multidimensional NMR and 3D structure calculation of biomolecules. Bioinformatics. 2021;37(18):3041-2.
43. Guntert P. Automated NMR structure calculation with CYANA. Methods Mol Biol. 2004;278:353-78.
44. Shen Y, Delaglio F, Cornilescu G, Bax A. TALOS+: a hybrid method for predicting protein backbone torsion angles from NMR chemical shifts. J Biomol NMR. 2009;44(4):213-23.
45. Buchko GW, Hewitt SN, Van Voorhis WC, Myler PJ. Solution NMR structures of oxidized and reduced Ehrlichia chaffeensis thioredoxin: NMR-invisible structure owing to backbone dynamics. Acta Crystallogr F Struct Biol Commun. 2018;74(Pt 1):46-56.
46. Bhattacharya A, Tejero R, Montelione GT. Evaluating protein structures determined by structural genomics consortia. Proteins. 2007;66(4):778-95.
47. Chadha S, Kale SP. Simple fluorescence-based high throughput cell viability assay for filamentous fungi. Lett Appl Microbiol. 2015;61(3):238-44.
48. Djami-Tchatchou AT, Tetorya M, Godwin J, Codjoe JM, Li H, Shah DM. Small Cationic Cysteine-Rich Defensin-Derived Antifungal Peptide Controls White Mold in Soybean. J Fungi (Basel). 2023;9(9).
49. Schindelin J, Arganda-Carreras I, Frise E, Kaynig V, Longair M, Pietzsch T, et al. Fiji: an open-source platform for biological-image analysis. Nat Methods. 2012;9(7):676-82.

Acknowledgements

The work presented here was supported by the National Science Foundation grant IOS-2037981 and the National Institute of Food and Agriculture GRANT13515963 to D.S and K.C. The structures for NCR13 were solved using resources at the W.R. Wiley Environmental Molecular Sciences Laboratory, a national scientific user facility sponsored by U.S. Department of Energy's Office of Biological and Environmental Research (BER) program located at Pacific Northwest National Laboratory (PNNL). Battelle operates PNNL for the U.S. Department of Energy. We also

acknowledge imaging support from the Advanced Bioimaging Laboratory (RRID:SCR_018951) at the Donald Danforth Plant Science Center (DDPSC) and usage of the Leica SPX-8 acquired through an NSF Major Research Instrumentation grant (DBI-1337680). We acknowledge the DDPSC Proteomics & Mass Spectrometry Facility and supported by the National Science Foundation under Grant No. DBI-1827534 for acquisition of the Orbitrap Fusion Lumos LC-MS/MS. The greenhouse and growth chamber space provided by the DDPSC Plant Growth Facility is acknowledged. We also thank Dr. Ruby Tiwari for providing her comments on this manuscript.

Author Contributions

K.C. and D.S. conceived the research. J.G., A.D-C., S.V., M.T., K.C., M.Z., G.B. and D.S. designed the research. J.G., A.D-C., S.V., M.T., A.P., R.K, M.Z. and G.B. conducted the experiments. J.G., A.D-C., S.V., M.T., K.C., M.Z., G.B. and D.S. analyzed and interpreted the results. J.G., G.B., K.C. and D.S. wrote the manuscript.

Competing interests. The authors declare no competing interests.

Data deposition: The coordinates of the NCR13 NMR structure have been deposited in the Protein Data Bank, www.rcsb.org 8ULM (NCR13_ PFV1) and 7TH8 (NCR13_ PFV2) and the NMR chemical shifts have been deposited in the BioMagResBank, www.bmrb.wisc.edu BMRB-31111 (oxidized NCR13_PFV1) and BMRB-30979 (oxidized NCR13_PFV2).